An abundant merozoite surface protein of *Plasmodium falciparum* modulates susceptibility to inhibitory antibodies

Isabelle G. Henshall[1], Jill Chmielewski[1], Dimuthu Angage[2], Ornella Romeo[1], Keng Heng Lai[1, 3], Kaitlin R. Turland[1, 3], Nicki Badii[2], Michael Foley[2, 4], Robin F. Anders[2], James Beeson[5, 6,7] and Danny W Wilson[1, 3, 5, *].

[1]Research Centre for Infectious Diseases, School of Biological Sciences, The University of Adelaide, Australia 5005

[2]Department of Biochemistry and Chemistry, La Trobe Institute for Molecular Sciences, La Trobe University, Victoria, Australia 3086

[3]Institute for Photonics and Advanced Sensing (IPAS), University of Adelaide, 5005, SA, Australia

[4]AdAlta, 15/2 Park Drive, Bundoora, Victoria, Australia 3083

[5]Burnet Institute, 85 Commercial Road, Melbourne 3004, Victoria, Australia

[6]Department of Infectious Diseases, University of Melbourne, Victoria, Australia

[7] School of Translational Medicine and Department of Microbiology, Monash University, Victoria, Australia

*Corresponding Author: danny.wilson@adelaide.edu.au

Abstract

Malaria merozoite surface proteins (MSPs), are thought to have important roles in red blood cell (RBC) invasion and their exposure on the parasite surface makes them attractive vaccine candidates. However, their role in invasion has not been directly demonstrated and their biological functions are unknown. One of the most abundant proteins is *Pf*MSP2, which is likely an ancestral protein that has been maintained in the *Plasmodium falciparum* lineage and is a focus of vaccine development, whose function remains unknown. Using CRISPR-Cas9 gene-editing, we removed *Pf*MSP2 from two different *P. falciparum* lines with no impact on parasite replication or phenotype *in vitro*, demonstrating that it is not essential for RBC

invasion. However, loss of *Pf*MSP2 led to increased inhibitory potency of antibodies targeting other merozoite proteins involved in invasion, particularly *Pf*AMA1. In a solid-phase model, increasing concentrations of *Pf*MSP2 protein reduced binding of different antibodies against *Pf*AMA1 in a dose dependent manner. These data suggest that *Pf*MSP2 can modulate the susceptibility of merozoites to protective inhibitory antibodies. The results of this study change our understanding of the potential functions of *Pf*MSP2 and establishes a new concept in malaria where a surface protein can reduce the protective efficacy of antibodies targeting a different antigen. These findings have important implications for understanding malaria immunity and informing vaccine development.

Introduction

Plasmodium falciparum malaria remains a global health challenge with over half a million deaths annually (World Health Organization, 2024). Worryingly, increasing parasite resistance to frontline antimalarials and mosquito insecticide resistance are decreasing the effectiveness of key control measures (World Health Organization, 2024). Development of the RTS,S and R21 vaccines targeting the *P. falciparum* circumsporozoite protein is a step forward for malaria vaccine development, however further improvements in vaccine efficacy and longevity are needed to protect those most at risk – children under 5 years – and enable malaria elimination (Beeson et al., 2019; Datoo et al., 2024; RTSS Clinical Trials Partnership, 2015). Understanding the function of vaccine targets remains important for prioritisation and optimisation of candidates in the development pipeline. Merozoites, the parasite stage that invades host red blood cells (RBCs), have long been targeted for vaccine development since successful blocking of merozoite invasion would prevent the repeated cycles of blood-stage parasite multiplication and associated disease. While much work has been done to understand the processes and steps required for merozoite invasion, only a few merozoite proteins have successfully had functions defined. To date, most vaccines based on merozoite antigens have demonstrated limited efficacy (Beeson et al., 2016) at least in part due to the extensive polymorphisms exhibited by many of these antigens.

The surface of the merozoite is covered in a fibril coat which is comprised of multiple proteins, broadly known as merozoite surface proteins (MSPs). These proteins have been proposed to mediate weak initial merozoite RBC contact (Bannister et al., 1986; Beeson et al., 2016; Cowman et al., 2017; Weiss et al., 2015) and in *P. falciparum* are dominated by GPI-anchored

proteins, the most abundant being *Pf*MSP1 and 2 (Gilson et al., 2006). *Pf*MSP1 has been suggested to have a role in merozoite attachment to the RBC (Li et al., 2004), but recent evidence instead suggests that it has a role in merozoite rupture from schizonts and cellular interaction studies using optical tweezers do not support a substantial role for this protein in RBC binding (Das et al., 2015; Kals et al., 2024), although it may have another function in invasion. These recent insights into *Pf*MSP1 function, the best studied MSP, highlight what little is known of MSPs and their roles in parasite survival.

P. falciparum merozoite surface protein 2 (*Pf*MSP2), a protein proposed to be essential for parasite growth (Sanders et al., 2006), has been of long-term interest as a vaccine candidate. *Pf*MSP2 is a ~28 kDa intrinsically disordered protein that has conserved N- and C- termini, along with a central variable region that defines two main allelic groups, 3D7-like and FC27-like (Adda et al., 2012). While *Pf*MSP2 was theorised to have a mechanical role in the early steps of invasion (Anders et al., 2010), there is minimal supporting evidence for this, in part due to the lack of tools to study *Pf*MSP2 function. Studies with recombinant proteins suggest that it is likely *Pf*MSP2 interacts with lipids and forms complexes with itself on the merozoite surface (Adda et al., 2009; Lu et al., 2019; Zhang et al., 2012). *Pf*MSP2 peptides have also been reported to bind the RBC and inhibit *P. falciparum* growth, which would support *Pf*MSP2 mediating merozoite-RBC interactions (Ocampo et al., 2003). Unlike the majority of the merozoite surface coat proteins, *Pf*MSP2 is not present in other malaria parasites that infect humans and has been postulated to have evolved specifically in the *Laverania* subgenus of *Plasmodium*, which includes *P. falciparum* (Black et al., 2002).

*Pf*MSP2 has been trialled in a vaccine (Combination B) combined with fragments of *Pf*MSP1 and *Pf*RESA. A Phase 1/2b trial of this vaccine showed efficacy in reducing the parasite burden in children, which was specific to the *Pf*MSP2 3D7-like allele used in the vaccine formulation (Genton et al., 2003). Vaccine-induced antibodies from clinical trials or experiments in animals have little or no inhibitory activity in standard growth inhibition assays (Boyle et al., 2015; McCarthy et al., 2011), but did show functional activity through the recruitment of complement, promoting opsonic phagocytosis and antibody-dependent cellular inhibition (Boyle et al., 2015; Feng et al., 2018; McCarthy et al., 2011). Naturally acquired antibodies are also known to target *Pf*MSP2 and have been linked to protection (Fowkes et al., 2010; Osier et al., 2010; Stanisic et al., 2009; Zerebinski et al., 2024). Studies have highlighted that it is the Fc-mediated functional activities of these naturally acquired *Pf*MSP2 antibodies, as opposed to direct blocking of *Pf*MSP2 protein function, that correlates best with protection (Boyle et

al., 2015, 2014; Osier et al., 2014; Reiling et al., 2019). While *Pf*MSP2 is a key target of naturally acquired malaria immunity, little is known about the function of *Pf*MSP2, hindering its advancement as a potential vaccine candidate.

Here we take a reverse genetics approach to assess the function of *Pf*MSP2, quantifying the impacts of *Pf*MSP2 deletion on parasite invasion and phenotype. Given our findings that deletion of MSP2 did not impact invasion *in vitro*, we tested the alternative hypothesis that merozoite surface proteins may function to modulate susceptibility of merozoites to inhibitory antibodies.

Results

Avian malaria MSP2-like proteins are structurally similar to *Laverania* MSP2s and show that MSP2 did not arise exclusively in this clade.

Genome annotations of *pfmsp2* show it lies between the merozoite surface protein *pfmsp5* (PF3D7_0206900) and *pfmsp*4 (PF3D7_0207000), and the conversed purine biosynthesis enzyme *adenylosuccinate lyase* (ADSL, PF3D7_0206700) (Figure 1A) (PlasmoDB; (Aurrecoechea et al., 2009)), with this arrangement previously thought to be restricted to the *Laverania* clade which includes parasites that infect great apes and *P. falciparum* (Black et al., 2002; Ferreira et al., 2015). As described by Escalante et al. (2022), we found the genomes of the two annotated avian *Plasmodium* spp. available on PlasmoDB, *P. relictum* and *P. gallinaceum*, to also have a putative gene between ADSL and MSP5 with structural similarities to *Laverania* MSP2s. The reduced length of the *P. relictum* (PRELSG_0415300) and *P. gallinaceum* (PGAL8A_00017700) MSP2-like proteins compared to those of *Laverania* parasites is accounted for by the absence of any extended central domains of the two avian malaria parasites (Supplementary Figure 1).

It is estimated that ~10 million years of evolution separate the avian malaria parasites *P. relictum* and *P. gallinaceum* from the *Laverania* (Böhme et al., 2018). Therefore, we explored whether similarities in amino acid sequence and predicted conformation would support a shared lineage and functional properties of MSP2 between *P. relictum* and *P. gallinaceum*

126 MSP2s with *Laverania* MSP2 sequences. The primary translation product of *Pf*MSP2 has
127 hydrophobic N- and C-terminal sequences that correspond to secretion signals (SP) and GPI-
128 attachment signals, respectively, which are absent from the mature polypeptide on the
129 merozoite surface. The putative SP (Supplementary Figure 1, Table 1) has an amino acid
130 similarity (BLSM62) of >89% across the *Laverania* and avian malaria parasites, whereas, the
131 C-terminal GPI signal sequences of ~24 residues shows >79% amino acid similarity and shared
132 hydrophobicity across the *Laverania* and avian malarias. Both *P. relictum* (Asp, Ala, Ser: based
133 on big-PI Predictor (Eisenhaber et al., 1999)) and *P. gallinaceum* (Asp, Gly Ala) MSP2s have
134 a sequence of three amino acids with short side chains immediately prior to this C-terminal
135 hydrophobic region which, although different to the conserved sequence seen with the
136 *Laverania* (Ser, Asn, Ile/Met (Smythe et al., 1991)), conforms to an amino acid sequence
137 expected for a GPI signal (Gilson et al., 2006) (Supplementary Figure 1). Typically, N-terminal
138 of a GPI cleavage site lies an unstructured linker region of up to 10 amino acids rich in polar
139 residues, as seen for *Laverania* MSP2s (polar residues: 50% 2 species to 70% 4 species). For
140 the *Laverania*, this region has almost no Acidic amino acids (Acidic residues: 0% 7 species to
141 10% 3 species) (Supplementary Figure 1, Table 1). In contrast, this region has reduced levels
142 of polar, but is enriched in acidic amino acids, for both *P. relictum* (20% polar, 40% acidic)
143 and *P. gallinaceum* (10% polar, 30% acidic). Although there are some differences in the N and
144 C-terminal regions between *P. relictum* and *P. gallinaceum* and the *Laverania* MSP2s, these
145 signal sequences are broadly conserved in properties which suggests a conserved sub-cellular
146 localisation.

147 Immediately downstream of the N-terminal SP lies the 24 amino acid N-terminal conserved
148 region (Supplementary Figure 2). This region of MSP2 has a propensity for alpha-helical
149 structure and fibril formation (Yang et al., 2010). Amino acid similarity through the N-terminal
150 conserved region is 78% across the *Laverania* and avian parasites, resulting in similar
151 proportions of hydrophobic, polar uncharged, basic and acidic amino acid across this region
152 (Table 1). Following the N-terminal conserved regions lies the dimorphic central variable
153 repeat region in *P. falciparum* MSP2s that are grouped as 3D7 or FC27-like amino acid
154 sequence structures. A defining feature of the 3D7-like MSP2 family are 4 or 8-mer tandem
155 repeats consisting of small amino acids (for 3D7: Gly, Gly, Ser, Ala) (MacRaild et al., 2015;
156 Smythe et al., 1991). The FC27-like MSP2 family also has repeats of 12 or 32 amino acids in
157 length, but these do not resemble those of the 3D7-like family. We found that the non-*P.*
158 *falciparum Laverania* and avian malaria MSP2 sequences compared consisted of >75% small

159 amino acids (some of: Gly, Ser, Ala, Thr) generally ordered in repeats downstream of the N-
160 terminal conserved region (Supplementary Figure 3). The number of repeats (4-repeats = 5
161 examples to 8 repeats = *P. relictum*), the length of the repeats (3-amino acids = 5 examples to
162 7-amino acids = *P. praefalciparum*) and whether the repeats were highly conserved or had
163 various levels of degeneracy (conserved = 4 examples to partially or highly degenerate = 10
164 examples) differed between and within species (Table 1, Supplementary Figure 3). A broader
165 search of an additional nine *Laverania* MSP2s identified from the NCBI experimental database
166 did not reveal any repeat or central variable regions that resembled FC27-like MSP2s (data not
167 shown). This comparison highlights the surprising finding that a region of known dimorphic
168 variability in *P. falciparum* MSP2 is likely to retain functional constraints that favour small
169 amino acid rich repeats immediately downstream of the N-terminal conserved region. Broadly
170 speaking, this groups the compared *Laverania* and avian malaria MSP2s as having a 3D7-like
171 repeat structure.

172 Upstream of the C-terminal GPI signal sequence lies the 50 amino acid residue C-terminal
173 conserved region (Supplementary Figure 4). This region contains two cysteine residues in all
174 *Laverania* MSP2s, which are thought to form an intramolecular disulphide bond (Zhang et al.,
175 2008). Two cysteine residues are present in the C-terminus of *P. gallinaceum*, but not *P.*
176 *relictum* MSP2 which has a single cysteine (Supplementary Figure 4). *Laverania* MSP2
177 similarity through the 50 residue sequence that makes up the C-terminal conserved region was
178 80%, with the hydrophobic residues making up between 20% (*P. billcollinsi*) and 34% (*P.*
179 *adleri*) of the amino acid content (Table 1). Amino acid similarity dropped to 62% when all
180 available C-terminal conserved domain residues were compared between *Laverania* and the
181 avian malarias due to the limited amino acid sequence similarity upstream of the cysteine
182 residue/s and apparent insertions of 20 (*P. relictum*) and 26 (*P. gallinaceum*) amino acids
183 downstream of the first Cysteine (Supplementary Figure 4). However, the percentage of
184 hydrophobic residues for *P. relictum* (33%) and *P. gallinaceum* (34%) was broadly in line with
185 that seen for the *Laverania*.

186 Extensive studies on recombinant proteins of the *P. falciparum* 3D7 and FC27 variants of
187 *Pf*MSP2 have shown this merozoite surface protein to be intrinsically disordered. Given the
188 evidence for conservation of the primary structure of MSP2s from distantly related malaria
189 parasites, we used AlphaFold2 predictions (Jumper et al., 2021) to examine whether there were
190 likely to be also conformational similarities between *Laverania* MSP2s and those of *P. relictum*
191 and *P. gallinaceum*. The MSP2s in the database of AlphaFold2-predicted structures retain their

192 N- and C-terminal signal sequences, but as these are both absent from mature MSP2 on the
193 merozoite surface they were deleted from the MSP2 sequences used for the AlphaFold2
194 predictions reported here. The predicted structures of the two avian parasite MSP2s, and other
195 *Laverania* MSP2s, are very similar to that of *Pf*3D7 MSP2, with most of the polypetide chains
196 lacking predicted secondary structure and, from the colour coding, have a predicted local
197 distance test (pLDDT) consistent with that of an intrinsically disordered protein over the
198 majority of the proteins length (Figure 1B). In contrast to the rest of the polypeptide, some α-
199 helical structure was predicted in the conserved 20-residue N-terminal region of all the
200 *Laverania* and avian MSP2s. NMR studies with recombinant *Pf*3D7 and *Pf*FC27 MSP2
201 showed this conserved N-terminal sequence to have a propensity for forming an α-helix that
202 was stabilized in the presence of lipid mimetics (MacRaild et al., 2012). The low pLDDT
203 values are consistent with this region in the other *Laverania* and *P. gallinaceum* MSP2 having
204 some propensity for α-helix formation, whereas higher pLDDT values suggest the possible
205 presence of a more stable α-helix in this region of *P. relictum* MSP2.

206 Having established that MSP2 is present across different *Plasmodium* lineages sharing similar
207 predicted amino acid compositions and structural features, the phylogenetic relationship
208 between annotated *Laverania* and putative avian malaria parasite MSP2s was examined. A
209 phylogenetic tree was generated based on alignments of representative sequences from each
210 species. MSP2 sequences from species belonging to the *Laverania* subgenus all grouped
211 together with two smaller clusters, corresponding to the known *Laverania* clade A and clade
212 B species (Figure 1C). As expected, *P. relictum* and *P. gallinaceum* MSP2 also group together.
213 The phylogenetic tree generated based on MSP2 sequences mirrors the proposed evolution of
214 *Plasmodium* spp. (Figure 1C). As postulated by Escalante et al. (2022) , these data suggest that
215 MSP2 was likely present in the ancestral *Plasmodium* parasite prior to the split of the
216 mammalian infecting *Plasmodium* spp. from those that infect birds and lizards. Given the
217 shared amino acid sequence and predicted conformational similarities, including the high levels
218 of intrinsically disordered sequence outside of the N- and C-terminal regions, the *P. relictum*
219 and *P. gallinaceum* MSP2-like proteins appear likely to contain enough properties to
220 potentially be functionally equivalent to *Laverania* MSP2s. This conservation of MSP2-like
221 proteins across different species suggests it has an important function.

222

223

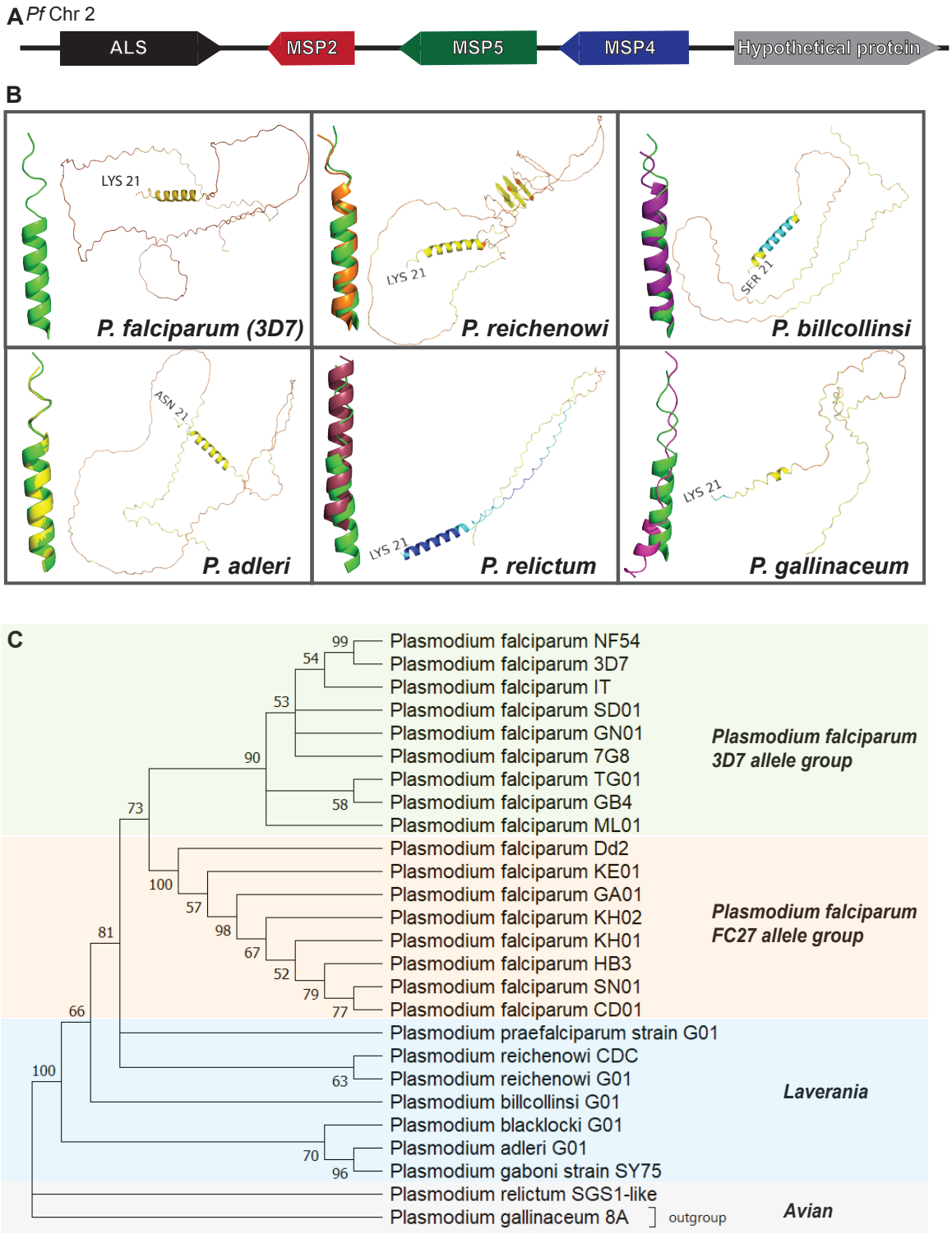
A Pf Chr 2
ALS
MSP2
MSP5
MSP4
Hypothetical protein
B
LYS 21
P. falciparum (3D7)
LYS 21
P. reichenowi
SER 21
P. billcollinsi
ASN 21
P. adleri
LYS 21
P. relictum
LYS 21
P. gallinaceum
C
Plasmodium falciparum NF54
Plasmodium falciparum 3D7
Plasmodium falciparum IT
Plasmodium falciparum SD01
Plasmodium falciparum GN01
Plasmodium falciparum 7G8
Plasmodium falciparum TG01
Plasmodium falciparum GB4
Plasmodium falciparum ML01
Plasmodium falciparum Dd2
Plasmodium falciparum KE01
Plasmodium falciparum GA01
Plasmodium falciparum KH02
Plasmodium falciparum KH01
Plasmodium falciparum HB3
Plasmodium falciparum SN01
Plasmodium falciparum CD01
Plasmodium praefalciparum strain G01
Plasmodium reichenowi CDC
Plasmodium reichenowi G01
Plasmodium billcollinsi G01
Plasmodium blacklocki G01
Plasmodium adleri G01
Plasmodium gaboni strain SY75
Plasmodium relictum SGS1-like
Plasmodium gallinaceum 8A
outgroup
Plasmodium falciparum 3D7 allele group
Plasmodium falciparum FC27 allele group
Laverania
Avian
99
54
53
90
58
73
100
57
98
67
52
79
77
81
66
100
63
70
96

224

225

226

227 **Figure 1.** Presence and structure of MSP2 across different *Plasmodium* species. **(A)** Schematic
228 of the gene arrangement surrounding *msp2* on *P. falciparum* chromosome 2. **(B)** AlphaFold2
229 structural predictions of example *Laverania* (*P. falciparum* (3D7), *P. reichenowi*, *P.*
230 *billcollinsi*, *P. adleri*) and the two avian (*P. relictum*, *P. gallinaceum*) malaria species. The N-
231 terminal signal peptide and C-terminal GPI anchor sequences were removed before the proteins
232 structure was predicted. The most N-terminal amino acid is indicated. Colours represent the
233 predicted local distance difference test (pLDDT) scores, with dark blue representing very high
234 confidence (>90%), light blue high confidence (90 to >70), yellow low confidence (70 to 50)
235 and orange very low confidence (<50). the Modelled structure of the N-terminal helical region
236 is provided as an inset for *P. falciparum* 3D7 MSP2 in isolation, and also in alignment with the
237 helical domain for *P. falciparum* 3D7 (green for all) for the other examples of *Laverania* and
238 avian MSPs (other colours). **(C)** Maximum likelihood tree showing relationship of MSP2
239 protein sequences found in different *P. falciparum* isolates and other *Plasmodium* species.
240 Grouping of sequences from *P. falciparum* isolates into two main allele types can be seen as
241 well as the separation of the *Laverania* and avian malaria species into their expected groups.
242 Tree robustness tested by bootstrap.

243

244 **Loss of *Pf*MSP2 does not noticeably impact growth or invasion of different *P. falciparum***
245 **lines *in vitro*.**

246 Given previous unsuccessful attempts to disrupt *pfmsp2* (Sanders et al., 2006), and its high
247 abundance on the merozoite surface (Gilson et al., 2006), *Pf*MSP2 has been traditionally
248 viewed as an essential *P. falciparum* protein with an essential function in merozoite invasion.
249 We employed CRISPR-Cas9 gene editing to determine whether the reported inability to knock-
250 out *pfmsp2 in vitro* was a result of this protein being essential for parasite survival or because
251 of the lower efficiency of the previously used gene-editing system (Sanders et al., 2006).
252 Unexpectedly, we confirmed successful disruption of *pfmsp2* by replacing the coding sequence
253 between 132 bp and 819 bp of the gene with a hDHFR drug selection cassette in the 3D7 *P.*
254 *falciparum* laboratory-adapted line (Figure 2A and B), resulting in *Pf*3D7 ΔMSP2 parasites.
255 We confirmed that *Pf*MSP2 was no longer expressed in *Pf*3D7 ΔMSP2 parasites by western
256 blot, which detected a MSP2 band around 50 kDa in *Pf*3D7 WT parasite material but not in
257 *Pf*3D7 ΔMSP2 parasites (Figure 2C). Similarly, immunofluorescence microscopy using anti-
258 *Pf*MSP2 rabbit polyclonal antibodies showed the expected surface localisation of MSP2 on

259 *Pf*3D7 WT merozoites but not on *Pf*3D7 ΔMSP2 parasites (Figure 2D). We next assessed
260 whether knock-out of *Pf*MSP2 impacted on parasite growth over one or two cycles of
261 development *in vitro* and found that deletion of *Pf*3D7 MSP2 did not cause any significant
262 change in growth (Figure 2E and F).

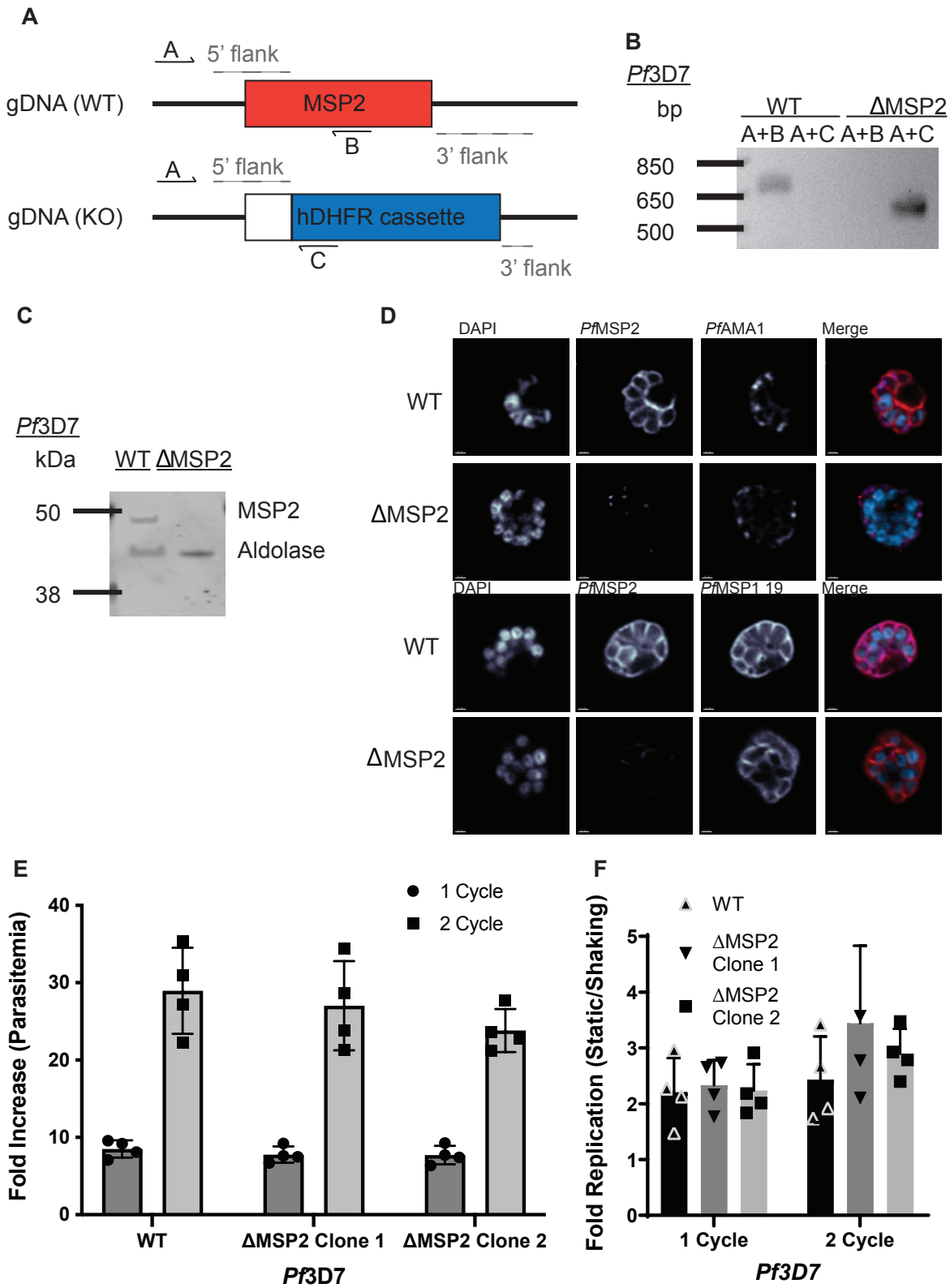

Figure 2. *Pf*MSP2 is not essential for growth *in vitro* of *Pf*3D7 blood stage parasites. **(A-B)** Schematic and agarose gel showing integration of knockout construct (band A+C) in the *msp2* gene locus and absence of the *msp2* sequence from the *Pf*3D7 ΔMSP2 line (band A+B).

267 **(C)** Western Blot of late schizont protein extracts confirms no *Pf*MSP2 is expressed in the
268 *Pf*3D7 ΔMSP2 line. *Pf*MSP2 detected by anti-*Pf*MSP2 2F2 3D7 mAb with *Pf*Aldolase
269 serving as loading control. Representative image shown. **(D)** Distribution of key merozoite
270 surface proteins in the presence or absence of *Pf*MSP2 was visualised by
271 immunofluorescence. *Pf*MSP2 (red for top two rows, purple in bottom two rows), the nucleus
272 stained by DAPI (blue in merge) and *Pf*AMA1 (purple, top two rows) or *Pf*MSP1 19 (red,
273 bottom two rows), and the coloured merge of the proceeding panels. Scale bar = 0.7 µm.
274 Representative images shown from a minimum of 10 schizonts imaged per condition. **(E-F)**
275 Growth of *Pf*3D7 WT compared to *Pf*3D7 ΔMSP2 *P. falciparum* parasites, measured as fold
276 increase in parasitaemia, over one (48 hrs) or two (96 hrs) cycles in either standard (still- (E))
277 or shaking (F) conditions. Parasitaemia was determined by flow cytometry at the start and
278 end to calculate fold increase. Graph displays mean ± S.D. of three independent experiments
279 performed with technical triplicates. Significance determined by unpaired t-test with $p < 0.05$
280 deemed significant.

281

282

283 As *Pf*MSP2 has been considered, to this point, as essential for *P. falciparum* growth *in vitro*
284 (Sanders et al., 2006), we investigated whether *Pf*MSP2 could also be removed from *Pf*Dd2,
285 an isolate of *P. falciparum* that differs from 3D7 in geographical origin, RBC receptor usage
286 and allelic type of *pfmsp2*. Using CRISPR-Cas9 we successfully knocked-out *msp2* in *Pf*Dd2
287 (Figure 3 A and B) and confirmed the absence of the protein in *Pf*Dd2 ΔMSP2 parasites using
288 western blot (Figure 3C). As we found for *Pf*3D7, deletion of *Pf*Dd2 *msp2* did not result in a
289 significant impact on parasite growth over one or two cycles of parasite replication (Figure
290 3D).

291 Given the abundance of *Pf*MSP2 on the merozoite surface, we postulated that loss of this
292 protein may impact on the timing of merozoite invasion of the RBC, which is not reflected in
293 reduced growth in *in vitro* cultures. Previous studies using live-cell microscopy have reported
294 that merozoites first contact the RBC and form weak initial interactions. The merozoite then
295 reorientates to bring apical organelles into position to release their contents onto the RBC,
296 which then leads to formation of the tight junction, merozoite invasion through the tight-
297 junction, formation of the parasitophorous vacuole and resealing of the RBC membrane post-
298 entry (Weiss et al., 2015). Given its surface localization, *Pf*MSP2 has been speculated to act in

299 the early phase of merozoite attachment. To assess whether knock-out of *pfmsp2* impacted on
300 the progression of invasion, we used live-cell microscopy of *Pf*Dd2 ΔMSP2 parasites and
301 compared the timing and key steps of invasion to *Pf*Dd2 WT parasites *in vitro*. This analysis
302 showed that *Pf*Dd2 ΔMSP2 knock-out parasites had no detectable alteration in the time the
303 parasite takes to attach to the RBC, the length or strength of RBC deformation as the merozoite
304 begins entry or for the time it took for invasion to be completed compared to *Pf*Dd2 WT (Figure
305 3 E-H). Together these data show *Pf*MSP2 is not essential for blood-stage replication *in vitro*
306 in two *P. falciparum* laboratory isolates from different geographical regions and knock-out of
307 *Pf*MSP2 does not seem to impact parasite growth or merozoite invasion *in vitro*. However, its
308 conservation across diverse *Plasmodium* spp. suggests it does play an important function or is
309 advantageous for parasite survival.

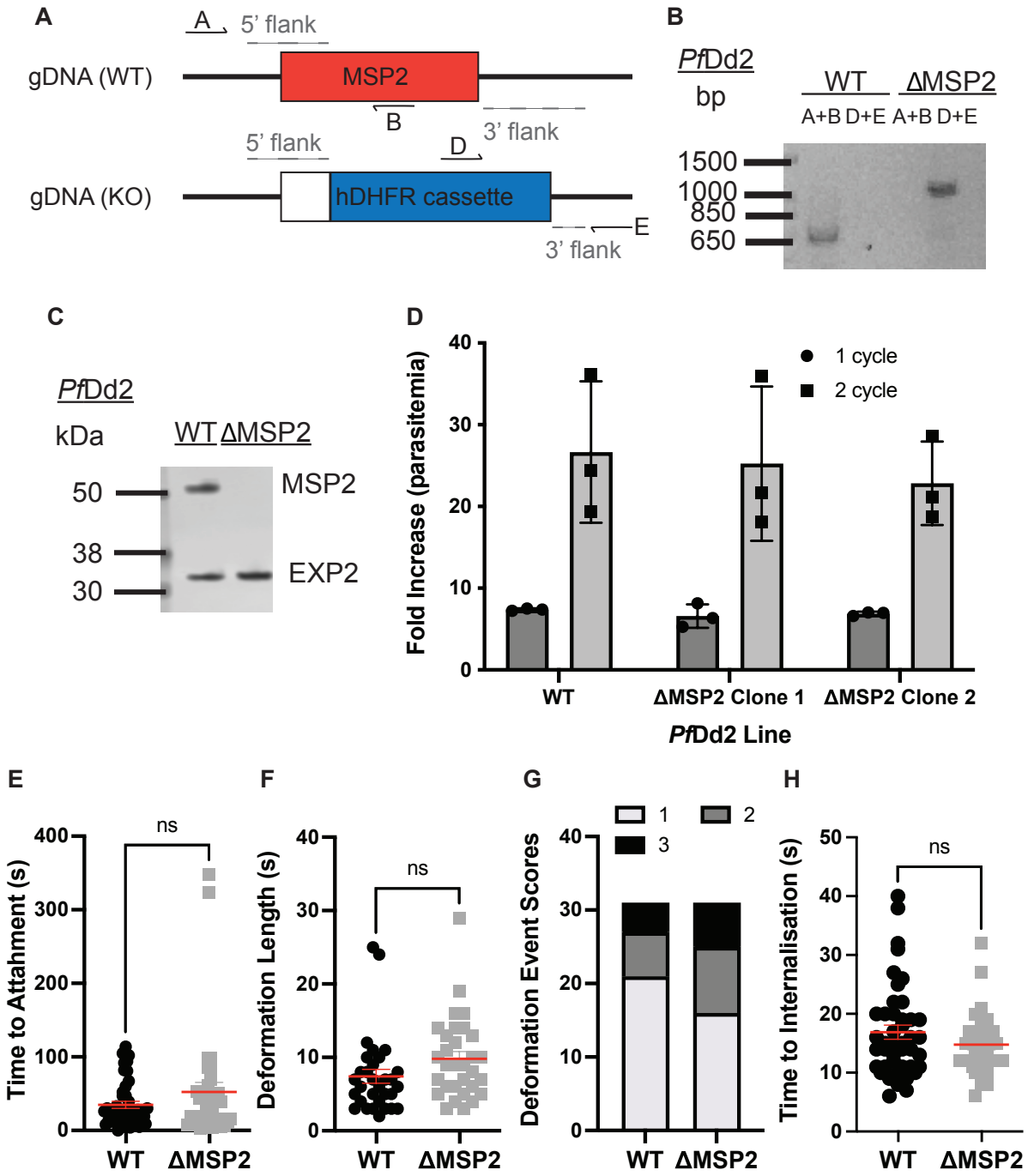
A
A
5' flank
gDNA (WT)
MSP2
B
3' flank
5' flank
D
gDNA (KO)
hDHFR cassette
E
3' flank
B
PfDd2
bp
WT
ΔMSP2
A+B D+E A+B D+E
1500
1000
850
650
C
PfDd2
kDa
WT ΔMSP2
50
38
30
MSP2
EXP2
D
Fold Increase (parasitemia)
1 cycle
2 cycle
WT
ΔMSP2 Clone 1
ΔMSP2 Clone 2
PfDd2 Line
E
Time to Attahment (s)
ns
WT
ΔMSP2
F
Deformation Length (s)
ns
WT
ΔMSP2
G
Deformation Event Scores
1
2
3
WT
ΔMSP2
H
Time to Internalisation (s)
ns
WT
ΔMSP2

311 **Figure 3.** *Pf*Dd2 does not require MSP2 for asexual growth *in vitro*. **(A-B)** Successful
312 integration of KO construct (schematic in A) into the *msp2* gene locus of *Pf*Dd2 ΔMSP2 was
313 confirmed by PCR of genomic DNA (primers A+B amplify WT locus, primers D+E amplify
314 integrated KO construct). **(C)** Loss of *Pf*MSP2 expression was demonstrated by western blot
315 of schizont protein extract with *Pf*MSP2 detected by anti-*Pf*MSP2 FC27 and anti-*Pf*EXP2 as
316 loading control. Representative image shown. **(D)** Growth of *Pf*Dd2 WT *P. falciparum*
317 parasites and *Pf*Dd2 ΔMSP2 over one (48 hrs) or two (96 hrs) cycles. Parasitaemia was
318 determined by flow cytometry at the start and end to calculate fold increase. Graph displays
319 mean ± S.D. of three independent experiments performed with technical triplicates. **(E-H)** Key
320 parameters of merozoite invasion were measured for both *Pf*Dd2 WT and *Pf*Dd2 ΔMSP2
321 parasites that had successfully invaded a RBC using live cell imaging of merozoite invasion.
322 Time to merozoite attachment to RBCs **(E)**, length **(F)** and strength **(G)** of RBC deformation,
323 and time to complete merozoite invasion **(H)** were measured by live microscopy. A minimum
324 of 30 invading merozoites for each line were captured and assessed. Significance determined
325 by unpaired t-test with $p < 0.05$ deemed significant.

326

327

328 **Impact of MSP2 gene deletion on gene expression and invasion pathway usage.**

329 Because of the close proximity of the *pfmsp*2, 4 and 5 genes on chromosome 2, similarities in
330 their structure (e.g. GPI-anchor intrinsically disordered protein) and shared merozoite surface
331 localization, we used qPCR to assess whether knock-out of *Pf*3D7 MSP2 impacted the
332 expression levels of *Pf*3D7 MSP4 or MSP5. We found no change in MSP4 and MSP5
333 expression levels between *Pf*3D7 ΔMSP2 parasites and *Pf*3D7 WT parasites (Figure 4A). As
334 expected, *Pf*MSP2 was not detected in the *Pf*3D7 ΔMSP2 parasites.

335 Secreted *P. falciparum* antigens belonging to the erythrocyte binding antigen (EBA) and
336 reticulocyte binding homologue (Rh) families are known to facilitate host-cell invasion through
337 specific receptors on the RBC surface. Reliance on specific EBA or Rh proteins, or their
338 cognate host-cell receptor, define different invasion pathways that can be crudely described by
339 the sensitivity of merozoite invasion to cleavage of RBC surface proteins with trypsin,
340 chymotrypsin and neuraminidase (Baum et al., 2005; Duraisingh et al., 2003; Orlandi et al.,
341 1992).When we assessed whether *Pf*MSP2 knock-out impacted merozoite invasion pathway

342 usage, we found that *Pf*3D7 ΔMSP2 parasites grew equally as well as *Pf*3D7 WT parasites in
343 all enzyme-treated RBCs (Figure 4B).

344 To investigate whether *Pf*MSP2 knock-out caused any changes in gene-expression of proteins
345 that may have a role in merozoite invasion and possibly compensate for loss of *Pf*MSP2, we
346 undertook RNA sequencing and differential gene expression analysis of *Pf*3D7 ΔMSP2 and
347 *Pf*3D7 WT parasites. As expected, the *Pf*MSP2 transcript, which was targeted for removal by
348 our CRISPR-Cas9 strategy, was not detected in the *Pf*3D7 ΔMSP2 parasites between 132 bp
349 and 819 bp (Supplementary Figure 5). After removal of genes belonging to variant surface
350 antigen families from the data, eight proteins were found to have a log2fold expression increase
351 above 1; none of these proteins are annotated as a merozoite surface or secreted protein linked
352 to merozoite invasion (Figure 4C, Table 2). Five of these eight upregulated proteins are of
353 unknown function and expressed at schizont stages, and only one (*Pf*3D7_0909100) has a
354 transmembrane domain that could possibly anchor it to a membrane surface as the GPI anchor
355 does for *Pf*MSP2 (Table 2). Three proteins were found to have a log2fold expression of <-1,
356 indicating a significant reduction in expression with *Pf*MSP2 knock-out, with *Pf*MSP2 being
357 one of these and the other two predicted to be exported proteins (Figure 4C, Table 2). While
358 these data do not exclude any of the *Plasmodium* proteins with unknown function that are
359 upregulated in *Pf*3D7 ΔMSP2 parasites as having a role that compensates for the loss of
360 *Pf*MSP2, only one is predicted to have a transmembrane domain that would bind it to a
361 membrane and no protein identified as up or down-regulated with *Pf*MSP2 knock-out has
362 previously been linked to merozoite invasion. Therefore, *Pf*MSP2 knock-out does appear to
363 have led to changes in gene expression, but does not appear to have a significant impact on the
364 regulation of known merozoite surface or secreted protein gene-expression that would suggest
365 loss of *Pf*MSP2 is compensated for by another protein.

366

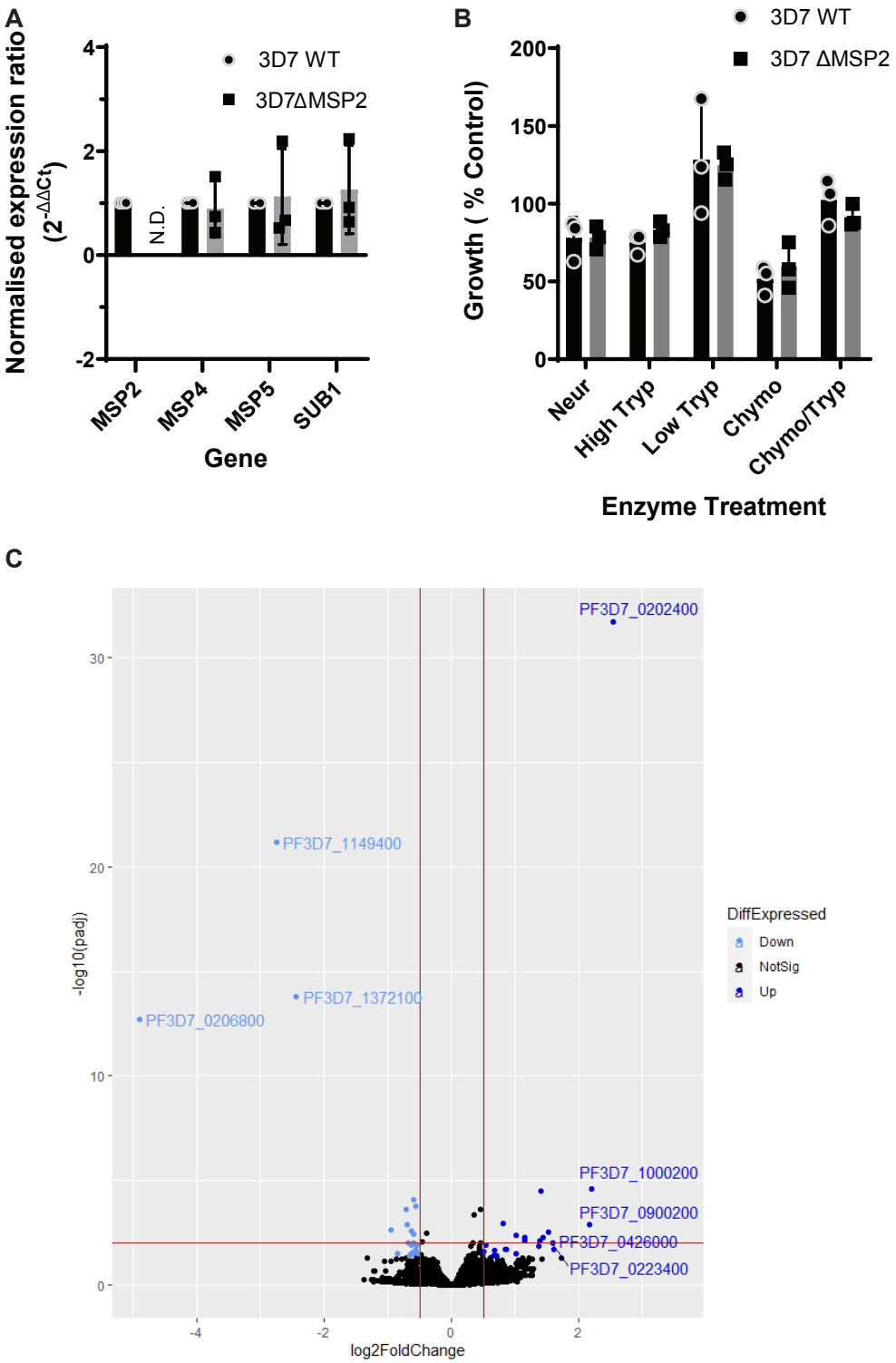

367

368 **Figure 4.** The impact of the loss of *Pf*MSP2 on expression of known merozoite invasion genes
369 and invasion pathway utilization. **(A)** Impact of *Pf*MSP2 KO on transcription during schizonts
370 was assessed by qPCR for genes located in proximity to *Pfmsp*2 on chromosome 2. Changes
371 in expression between *Pf*3D7 WT and *Pf*3D7 ΔMSP2 parasites was determined by qPCR

372 relative to *pfaldolase* expression with *pfsub1* serving as a schizont stage control. Graph displays
373 mean ± S.D. of three independent RNA harvests. **(B)** Selective enzymatic cleavage of key RBC
374 receptors showed no difference in invasion preference between *Pf*3D7MSP2 WT and *Pf*3D7
375 ΔMSP2 parasites. Parasitaemia was determined by flow cytometry and compared to growth in
376 non-treated control RBCs. Graph displays mean ± S.D. of three independent experiments. **(C)**
377 Log2(fold change) for differentially expressed genes, including multigene families, between
378 the transcriptome of *Pf*3D7 WT and *Pf*3D7 ΔMSP2 schizonts. Black lines differentiate genes
379 with a log2 (fold change) > 0.5 and < -0.5 with adjusted p-value < 0.05. Four independent
380 schizont RNA harvests were performed and analysed. Significance determined by t-test with
381 p< 0.05 deemed significant.

382

383 **Impact of *Pf*MSP2 disruption on antibodies and inhibitors targeting secreted surface**
384 **exposed antigens**

385 Merozoites are key targets of antibodies during malaria infection with antibodies either able to
386 directly block protein function and thus merozoite invasion, or recruit effectors such as
387 complement leading to the destruction of the merozoite (Beeson et al., 2016). Given the
388 prominence of *Pf*MSP2 on the merozoite surface we asked the question; how does the loss of
389 *Pf*MSP2 affect antibody efficacy against merozoites?

390 *Pf*EBAs and *Pf*Rhs moderate early steps in invasion with a degree of redundancy between these
391 proteins. Several EBAs and Rhs can be targeted with invasion inhibitory antibodies and are
392 targets of acquired human antibodies (Persson et al., 2013, 2008; Richards et al., 2013). We
393 found no significant difference in the ability of purified rabbit immunoglobulin raised against
394 single (*Pf*Rh2b) or combinations of *Pf*EBAs and *Pf*Rhs (*Pf*EBA175/*Pf*Rh2b,
395 *Pf*EBA175/*Pf*Rh4, *Pf*EBA175/*Pf*Rh2b/*Pf*Rh4) to inhibit growth of *Pf*3D7 WT or *Pf*3D7
396 ΔMSP2 parasites (Figure 5A). Similarly, knock-out of MSP2 in *Pf*Dd2 did not significantly
397 change the parasites sensitivity to rabbit antibodies raised against isogeneic W2mef EBA175
398 (Figure 5B). Broadly speaking, these results mirror what was seen with selective cleavage of
399 the RBC ligands of *Pf*EBAs and *Pf*Rhs using enzyme treatment of RBCs (Figure 4B), with no
400 evidence that loss of *Pf*MSP2 changed either the importance of these secreted merozoite
401 antigens during invasion or their sensitivity to antibodies targeting different antigens.

402 The interaction of *Pf*Rh5 with RBC surface receptor basigin is a critical, non-redundant
403 interaction for *P. falciparum* merozoite invasion and a known target of direct invasion-

404 inhibitory antibodies (Alanine et al., 2019; Crosnier et al., 2011; Douglas et al., 2011). *Pf*Rh5
405 was the initial member of the PCRCR complex to be described, with subsequent studies
406 demonstrating that antibodies against other members of this complex could also block
407 merozoite invasion of the RBC (Scally et al., 2022). Given the importance of these secreted
408 antigens to current vaccine development efforts, we next investigated whether loss of *Pf*MSP2
409 impacted on the parasite's sensitivity to antibodies targeting these antigens. There was no
410 difference in sensitivity between *Pf*3D7 WT and *Pf*3D7 ΔMSP2 parasites when treated with
411 invasion-inhibitory rabbit antibodies targeting *Pf*Rh5 (Figure 5C) or nanobodies targeting
412 PCRCR complex component *Pf*PTRAMP (H8) (Figure 5D). Nanobodies targeting the PCRCR
413 complex component CSS (D2) showed a slight, but non-significant increase in invasion-
414 inhibitory activity in the absence of *Pf*MSP2 (1.4-fold increase; IC_{50} value for *Pf*3D7 WT is 57
415 μg/mL; IC_{50} value for *Pf*3D7 ΔMSP2 is 42 μg/mL; p=0.3; Figure 5E). However, the *Pf*3D7
416 ΔMSP2 specific increase in invasion-inhibitory activity was amplified with the addition of the
417 human Fc domain to the anti-CSS nanobody (D2-Fc) to be 3-fold greater for *Pf*3D7 ΔMSP2
418 parasites (IC_{50} *Pf*3D7 WT 138 μg/mL; IC_{50} *Pf*3D7 ΔMSP2 46 μg/mL; p=0.0001; Figure 5F).

419 The glycosaminoglycan heparin is a specific inhibitor of invasion and has been observed to
420 bind to the 42 kDa C-terminal region of *Pf*MSP1 the most abundant GPI-anchored protein on
421 the merozoite surface, marking this as a possible mechanism for its invasion inhibitory activity
422 (Boyle et al., 2010a). However, the highly charged state of heparin means that it could block
423 invasion through binding additional proteins. When tested against *Pf*3D7 WT and *Pf*3D7
424 ΔMSP2 parasites, we observed a small increase in inhibitory potency of heparin for parasites
425 lacking *Pf*MSP2 (1.4-fold; IC_{50} *Pf*3D7 WT 0.65 IU/mL; IC_{50} *Pf*3D7 ΔMSP2 0.47 IU/mL;
426 p=0.0003; Figure 5G). We next tested rabbit antibodies raised against the C-terminal 19 kDa
427 fragment of *Pf*MSP1. We found a small but non-significant trend towards increased inhibition
428 of growth in parasites that lacked *Pf*MSP2 across repeat experiments (Figure 5H). These data
429 suggest that loss of *Pf*MSP2 can impact on the invasion-inhibitory potency of some antibodies
430 that target secreted or surface antigens.

431

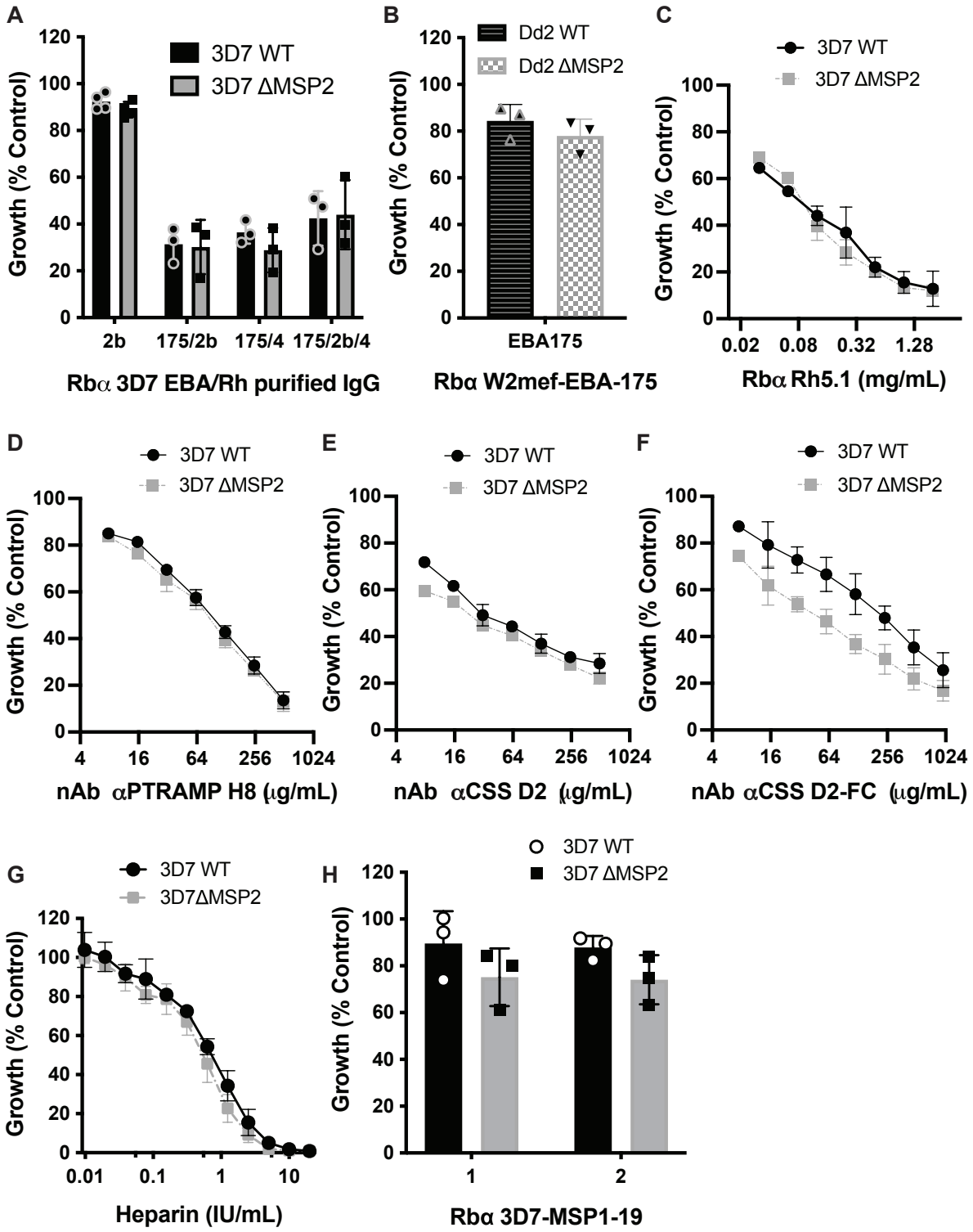
A
3D7 WT
3D7 ΔMSP2
Growth (% Control)
2b
175/2b
175/4
175/2b/4
Rbα 3D7 EBA/Rh purified IgG
B
Dd2 WT
Dd2 ΔMSP2
Growth (% Control)
EBA175
Rbα W2mef-EBA-175
C
3D7 WT
3D7 ΔMSP2
Growth (% Control)
Rbα Rh5.1 (mg/mL)
D
3D7 WT
3D7 ΔMSP2
Growth (% Control)
nAb αPTRAMP H8 (μg/mL)
E
3D7 WT
3D7 ΔMSP2
Growth (% Control)
nAb αCSS D2 (μg/mL)
F
3D7 WT
3D7 ΔMSP2
Growth (% Control)
nAb αCSS D2-FC (μg/mL)
G
3D7 WT
3D7ΔMSP2
Growth (% Control)
Heparin (IU/mL)
H
3D7 WT
3D7 ΔMSP2
Growth (% Control)
Rbα 3D7-MSP1-19

432

433

434 **Figure 5.** Impact of *Pf*MSP2 removal on efficacy of antibodies targeting other merozoite
435 surface-exposed antigens. Changes in antibody efficacy in the absence of *Pf*MSP2 was
436 assessed by measuring changes in antibody invasion inhibition and subsequent growth
437 compared to growth in the absence of antibody for both *P. falciparum* WT and ΔMSP2
438 parasites over 2 cycles. **(A)** Rabbit (Rb) IgG raised against merozoite antigens of the *Pf*3D7
439 EBA/Rh family. **(B)** Rabbit sera raised against *Pf*Dd2 EBA175. **(C)** Rabbit IgG raised against
440 *Pf*3D7 Rh5. **(D)** Nanobody (nAb) to *Pf*3D7 PTRAMP. **(E-F)** Nanobody and Fc-tagged
441 nanobody to *Pf*3D7 CSS. **(G)** The invasion inhibitory glycosaminoglycan heparin. **(H)** Rabbit
442 sera raised against *Pf*3D7 MSP1-19 (different vaccinated rabbit sera identified by numbers).
443 Graph displays mean ± S.D. of three different experiments. Significance was determined by
444 unpaired t-test when only a single concentration point was tested and for IC_{50} comparisons an
445 extra Sum-of-Squares F Test (best-fit $LogIC_{50}$) was performed with $p< 0.05$ deemed
446 significant.

447

448

449 **Loss of *Pf*MSP2 consistently potentiates AMA1 invasion inhibitory antibodies**

450 Subsequent to *Pf*Rh5 -basigin binding in the steps of merozoite invasion is the formation of the
451 tight-junction between *Pf*AMA1, secreted from the micronemes onto the merozoite surface,
452 and the rhoptry neck protein *Pf*RON2, which is inserted into the RBC membrane (Lamarque
453 et al., 2011; Srinivasan et al., 2011). In lines where *Pf*MSP2 was disrupted, we found a
454 consistent potentiation of antibodies that had anti-*Pf*AMA1 invasion-inhibitory activity.
455 Invasion-inhibitory polyclonal rabbit serum antibodies and purified immunoglobulin raised
456 against *Pf*AMA1 of *Pf*3D7 and *Pf*W2mef (isogenic to *Pf*Dd2), which express different alleles
457 of both *Pf*MSP2 and *Pf*AMA1, were found to be more inhibitory with *Pf*MSP2 knock-out
458 (Figure 6A and B). The polyclonal antibody with the greatest potentiation of inhibitory activity
459 was an IgG preparation purified from a rabbit antiserum raised against *Pf*W2mef AMA1. This
460 had a 3-fold increased potency against *Pf*Dd2 ΔMSP2 compared to *Pf*Dd2 WT (IC_{50} *Pf*Dd2
461 WT 0.015 mg/mL; IC_{50} *Pf*Dd2 ΔMSP2 0.005 mg/mL; $p<0.0001$) over two cycles of growth
462 (Figure 6B, C).

463 The mouse 1F9 (binds to the RON2 binding pocket and polymorphic loop 1d (Coley et al.,
464 2007)) and rat 4G2 (binds to a conserved epitope in the ectodomain (Kocken et al., 1998))
465 monoclonal antibodies have been shown to target different regions of *Pf*AMA1 and exhibit

466 selective inhibition against *Pf*3D7 AMA1. Here we found potentiation of invasion inhibitory
467 activity with *Pf*3D7 MSP2 knock-out for both 1F9 (2.1-fold; IC_{50} *Pf*3D7 WT 0.27 mg/mL; IC_{50}
468 *Pf*3D7 ΔMSP2 0.13 mg/mL; $p<0.0001$; Figure 6D) and 4G2 (3.2-fold; IC_{50} *Pf*3D7 WT 1.15
469 mg/mL; IC_{50} *Pf*3D7 ΔMSP2 0.36 mg/mL; $p<0.0001$; Figure 6E).

470 We also tested the invasion inhibitory effect of i-bodies, which are smaller single-domain
471 antibody-like molecules inspired from the shark variable new antigen receptor (V_{NAR})
472 (Griffiths et al., 2018, 2016). When we tested the i-body WD34 (Angage et al., 2024) which
473 binds a highly conserved epitope that includes the *Pf*RON2-binding pocket on *Pf*AMA1, we
474 observed a small potentiation of *Pf*AMA1 specific activity with knock-out of *Pf*MSP2 in *Pf*3D7
475 (1.3-fold; IC_{50} *Pf*3D7 WT 0.012 mg/mL; IC_{50} *Pf*3D7 ΔMSP2 0.009 mg/mL; $p=0.08$ Figure 6F).
476 Given WD34 was also found to be inhibitory to growth of W2mef parasites (Angage et al.,
477 2024) we also tested its activity against our *Pf*Dd2 ΔMSP2 parasites and found potentiation of
478 invasion inhibitory activity with loss of MSP2 in *Pf*Dd2 parasites (2-fold; IC_{50} *Pf*Dd2 WT
479 0.016 mg/mL; IC_{50} *Pf*Dd2 ΔMSP2 0.008 mg/mL; $p=0.004$ Figure 6G). As was observed for
480 the anti-CSS nanobody, addition of a human Fc domain to WD34 amplified the inhibitory
481 phenotype, with WD34 Fc having a 2.3-fold greater inhibitory activity against *Pf*3D7 ΔMSP2
482 than against *Pf*3D7 WT (IC_{50} *Pf*3D7 WT 0.1 mg/mL; IC_{50} *Pf*3D7 ΔMSP2 0.04 mg/mL;
483 $p=0.0004$; Figure 6H). A second i-body, WD33 (Angage et al., 2024), which binds AMA1
484 between domain II and domain III, had very limited invasion inhibitory activity against *Pf*3D7
485 parasites and did not show improved potency with knock-out of *Pf*3D7 MSP2 (0.9-fold; IC_{50}
486 *Pf*3D7 WT 1.02 mg/mL; IC_{50} *Pf*3D7 ΔMSP2 1.1 mg/mL; $p=0.8$; Figure 6I). Although the
487 limited inhibitory activity for WD33 tagged with the Fc receptor prevented us determining an
488 IC_{50} at the concentrations feasible to test, there was no increased inhibition of *Pf*3D7 ΔMSP2
489 parasites compared to the low level seen with *Pf*3D7 WT parasites (data not shown). These
490 data suggest that the potentiation of *Pf*AMA1 targeted antibody inhibition with MSP2 knock-
491 out is *Pf*AMA1 epitope dependent.

492 To account for the differences in i-body sizes, we compared the WD34 and WD34 Fc i-bodies
493 on a molar basis and found that they had similar activities against *Pf*3D7 MSP2 WT parasites
494 (IC_{50} 0.94 μM and 1 μM respectively) indicating that the Fc-tag itself did not modify epitope
495 binding properties. Rather, it is the absence of *Pf*MSP2 that results in increased inhibition of
496 AMA1 function by WD34, and this is further potentiated by antibody size.

497 In light of these results, we hypothesised that removal of *Pf*MSP2 may improve antibody access
498 to other antigens that are targets of inhibitory antibodies. To assess whether this was the case,
499 we first tested whether increased *Pf*AMA1 polyclonal antibody binding to the surface of
500 merozoites could be observed for *Pf*3D7 ΔMSP2 compared to *Pf*3D7 MSP2 WT parasites using
501 a fluorescently tagged WD34 i-body (WD34-mCherry) for quantitative immunofluorescence
502 assays of late stage schizonts labelled with a single incubation and wash step. We observed
503 WD34-mCherry to have a significantly higher mean fluorescence intensity for *Pf*3D7 ΔMSP2
504 compared to *Pf*3D7 WT (Figure 7A), supporting that the *Pf*AMA1 i-bodies may have better
505 access in the absence of *Pf*MSP2. As a control, we tested labelling using a fluorescently tagged
506 WD33 i-body which binds to AMA1 (Angage et al., 2024), but we found did not have improved
507 inhibitory activity in the absence of MSP2 (Figure 6I). Mirroring the results of the growth
508 assay, there was no difference observed for WD33-eGFP binding fluorescence for *Pf*3D7
509 ΔMSP2 compared to *Pf*3D7 WT parasites (Figure 7B).

510 We next explored whether the addition of recombinant *Pf*MSP2 could impact on the inhibitory
511 antibody binding on-rate against substrate-bound *Pf*AMA1 recombinant protein using Surface
512 Plasmon Resonance (SPR). For the anti-*Pf*AMA1 targeting mAb 4G2, there was a non-
513 significant trend toward a lower on-rate in the presence of recombinant *Pf*MSP2 (Figure 7C).
514 For the i-body WD34-Fc, there was minimal difference in detectable *Pf*AMA1 binding to
515 *Pf*AMA1 in the presence or absence of *Pf*MSP2 (Figure 7C). Using a similar principle of
516 testing antibody binding to substrate-bound *Pf*AMA1 protein in the presence, or absence of
517 increasing concentrations of *Pf*MSP2, we assessed changes in levels of anti-*Pf*AMA1 antibody
518 binding using an enzyme linked immunosorbent assay (ELISA). With increasing
519 concentrations of *Pf*MSP2 added to wells coated with AMA1, we found decreased binding of
520 anti-*Pf*AMA1 mAb 4G2 and i-body WD34-Fc by ELISA (Figure 7D). Interestingly, *Pf*MSP2
521 concentrations ≤0.31 μg/mL, an antigen concentration below the level that could be detected
522 by an MSP2 mAb, were enough to impact on the binding of *Pf*AMA1 antibodies. By looking
523 at the impacts of removing *Pf*MSP2 from the merozoite surface, or adding this protein in to
524 recombinant assays, these data provide additional support that inhibitory antibodies targeting
525 *Pf*AMA1 bind at a higher rate in the absence of *Pf*MSP2.

526

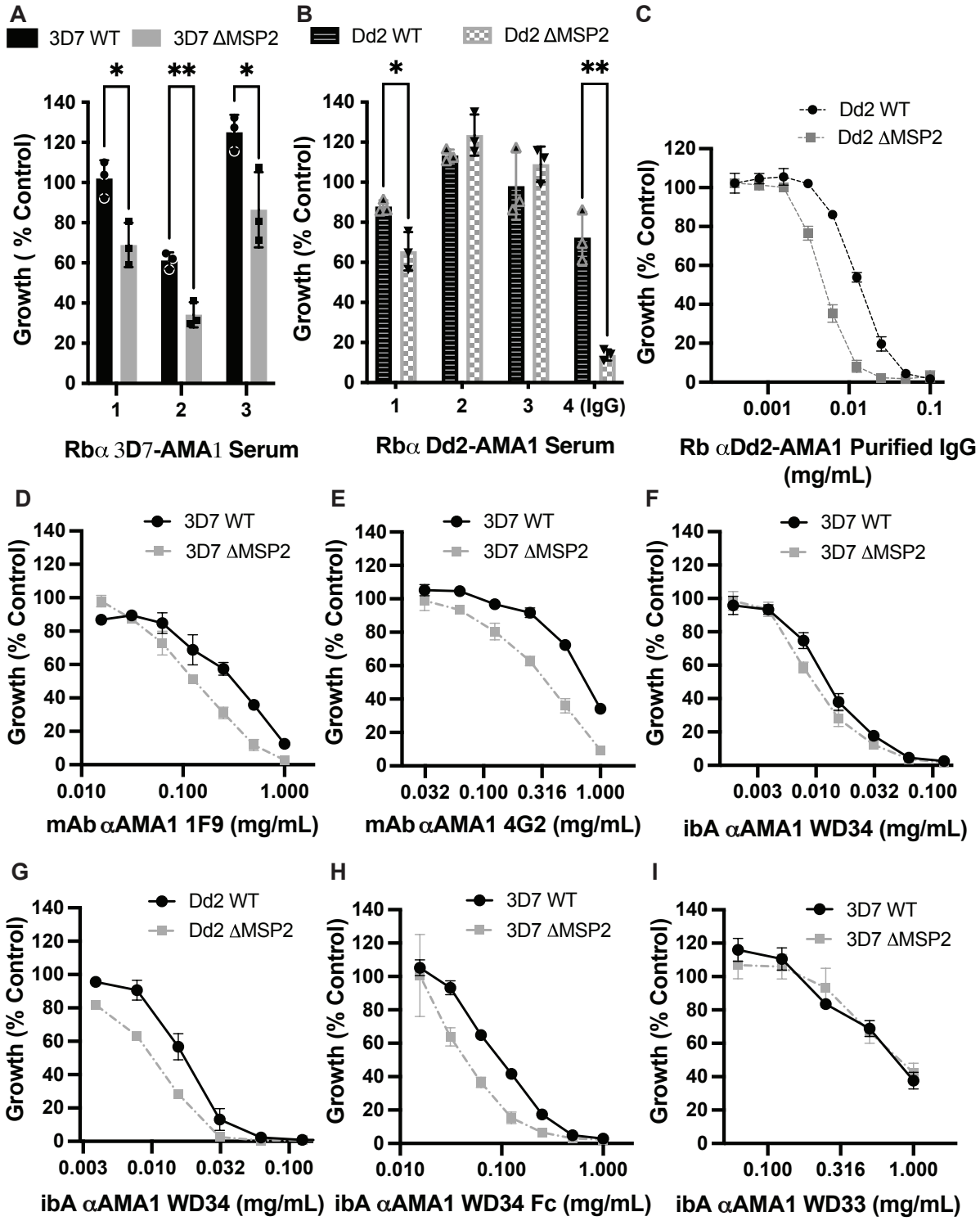

527

528 **Figure 6.** Absence of *Pf*MSP2 from the merozoite surface impacts invasion inhibition by

529 *Pf*AMA1 antibodies. *Pf*3D7 **(A, D-F, H, I)** and *Pf*Dd2 **(B, C, G)** express different *Pf*MSP2

530 alleles and different *Pf*AMA1 alleles, yet both showed altered anti-AMA1 antibody growth
531 inhibition in the absence of *Pf*MSP2. The effect was seen with serum (**A-B**; different
532 vaccinated rabbit (Rb) sera identified by numbers), purified rabbit and mouse monoclonal
533 (mAb) antibodies **(C-E)** and i-bodies (ibA) **(F-J)**. Final parasitaemia was determined by flow
534 cytometry and compared to control. Graph displays mean ± S.D. of three or four independent
535 experiments. Significance was determined by unpaired t-test when only a single concentration
536 point was tested and for IC_{50} comparisons an extra Sum-of-Squares F Test (best-fit $LogIC_{50}$)
537 was performed with $p < 0.05$ deemed significant.

538

539

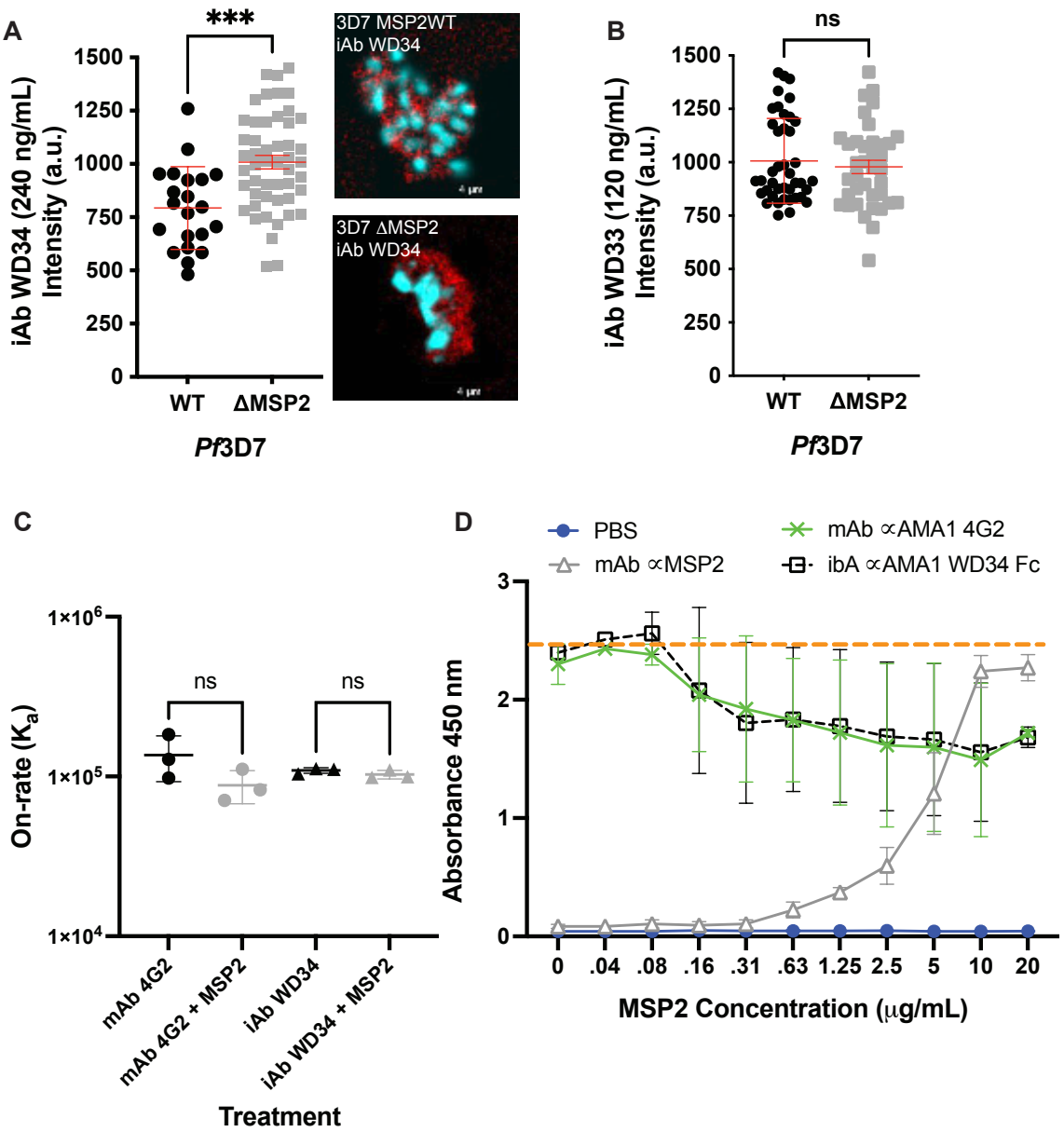

Figure 7. Quantitative fluorescence microscopy to assess whether differential binding may explain the increased potency of anti-*Pf*AMA1 invasion-inhibitory antibodies in the absence of *Pf*MSP2. Fluorescence intensity of fluorescently tagged anti-*Pf*AMA1 i-body (ibA) WD34-mCherry **(A)** and WD33-eGFP **(B)** for both *Pf*3D7 WT and *Pf*3D7 ΔMSP2, with a representative image for i-body WD34-mCherry. Nucleus in blue, i-body signal in red. Scale bar = 4 µm. Two independent experiments were performed with significance determined by unpaired t-test with $p < 0.05$ deemed significant. The lower overall mCherry signal required a higher antibody concentration (240 ng/mL) to have a comparable intensity measure to the eGFP tagged antibody (120 ng/mL) for *Pf*3D7 WT merozoites. **(C)** Read-out of the Surface plasmon resonance (SPR) antibody on-rate (association constant) for anti-*Pf*AMA1 mAb 4G2

551 and i-body WD34-Fc binding to *Pf*AMA1 in the presence or absence of *Pf*MSP2 protein.
552 Data represents the mean of 3 experiments with significance determined by unpaired t-test
553 with $p < 0.05$ deemed significant. **(D)** ELISA based assessment of the anti-*Pf*AMA1 mAb
554 4G2 and i-body WD34-Fc antibody binding levels to recombinant *Pf*3D7 AMA1 in the
555 presence or absence of recombinant *Pf*3D7 MSP2. PBS control demonstrates background
556 fluorescence. Dashed orange line provides a guide for peak absorbance levels. Anti-*Pf*MSP2
557 mAb shows increasing concentrations of *Pf*MSP2 protein results in decreased binding of
558 mAb 4G2 and i-body WD34-Fc. Data represents the mean of 3 experiments and error bars
559 are ±S.D.

560

561

562

563 **Discussion**

564 Despite decades of research and interest, the function of most merozoite surface proteins
565 remains unclear and targeting merozoite antigens in vaccine development has not achieved
566 high efficacy in clinical trials. Additionally, it has generally proven difficult to generate highly
567 inhibitory antibodies through vaccination with merozoite antigens. *Pf*MSP2 is one of the most
568 abundant proteins on the merozoite surface, has shown promise as a vaccine candidate and is
569 an established target of protective cytophilic antibodies (Boyle et al., 2015; Genton et al., 2002;
570 McCarthy et al., 2011; Osier et al., 2014, 2010). However, its function remains unclear. Our
571 findings here suggest that *Pf*MSP2 does not have an essential role in invasion *in vitro*, but can
572 modulate the sensitivity of merozoites to inhibitory antibodies targeting other antigens.

573 Despite its abundance on the merozoite surface and previous work suggesting a role in RBC
574 invasion, we found merozoites invade normally in the absence of this protein after gene
575 deletion. This does not exclude a role for *Pf*MSP2 *in vivo* where there are additional pressures,
576 such as immune-effector mechanisms and flow dynamics, on merozoite invasion. However,
577 given we have knocked-out *Pf*MSP2 from two different *P. falciparum* isolates, our findings do
578 not currently support a major role for *Pf*MSP2 in the mechanics of merozoite invasion. Thus,
579 it appears that the function of the two most abundant proteins on the merozoite surface,
580 *Pf*MSP1 (Das et al., 2015; Kals et al., 2024) and *Pf*MSP2, are not directly linked to merozoite
581 binding to the RBC and subsequent invasion. Deletion of MSP2 did lead to significant changes
582 in the expression of several genes, but there were no proteins with a clear link to merozoite

583 invasion and the biological relevance of these changes is not currently understood and requires
584 future investigation.

585 Both rabbit polyclonal and mouse monoclonal anti-*Pf*AMA1 antibodies tested were
586 consistently more inhibitory in the absence of *Pf*MSP2. Of the two *Pf*AMA1 targeting i-bodies
587 tested (Angage et al., 2024), the most potent WD34 was also more potent in the absence of
588 *Pf*MSP2, with this activity increasing significantly with the ~5.6-fold increase in size that
589 occurred upon addition of a mouse Fc region. Similarly, activity of a nanobody targeting the
590 PCRCR complex protein CSS showed increased potency in the absence of *Pf*MSP2, and again
591 this was increased further with antibody enlargement through addition of an Fc region. These
592 data suggest that *Pf*MSP2 may act to dampen the inhibitory activity of antibodies targeting
593 other antigens on the surface of the merozoite. Such immune dampening (called
594 conformational masking) by intrinsically disordered proteins, or protein regions, of host-cell
595 invasion related proteins has recently been demonstrated by modelling and gene-editing studies
596 in the viral pathogens HIV and HCV, respectively (Li et al., 2024; Stejskal et al., 2022). These
597 studies, along with our demonstration of increase antibody inhibitory efficacy with loss of the
598 intrinsically disordered *Pf*MSP2, support that this may be a widespread approach used by
599 pathogens to protect important protein functional sites from inhibitory antibodies.

600 A role in immune evasion has previously been suggested for *Pf*MSP2 and speculatively an
601 alternate explanation for the sensitisation observed is that this protein may shield key *Pf*AMA1
602 epitopes from antibody inhibition. For the *P. falciparum* 3D7 line, we found that *Pf*MSP2
603 knock-out led to higher *Pf*AMA1 binding as measured by increased fluorescence intensity for
604 the mCherry tagged i-body WD34 in the absence of *Pf*MSP2. Using a solid-phase model and
605 titrating recombinant *Pf*MSP2, we found that increasing concentrations of *Pf*MSP2 reduced
606 binding of an anti-*Pf*AMA1 mAb and i-body, even at concentrations where *Pf*MSP2 was not
607 detectable itself by antibodies. These data support that the presence of *Pf*MSP2 may reduce
608 antibody access (masking) to important invasion proteins exposed on the merozoites surface.
609 However, we acknowledge that the antibody-binding assays used (immunofluorescence assays,
610 SPR, ELISA) might not be sensitive enough to observe all potential changes in binding,
611 temporal changes when binding epitopes are exposed or differences in avidity that could lead
612 to increased antibody potency during the course of parasite invasion and growth, and these
613 factors may also contribute. Future studies of the merozoite surface and interactions between
614 proteins may help decipher in full how *Pf*MSP2 is protecting essential merozoite antigens from
615 invasion inhibitory antibody activity and reveal strategies for enhanced vaccine design.

616 Our observation that loss of *Pf*MSP2 potentiates the invasion-inhibitory activity of antibodies
617 targeting other antigens opens an additional avenue for vaccine development, such as targeting
618 *Pf*MSP2 to interfere with its potential role in immune evasion and thus potentiating antibodies
619 against other merozoite antigens. Additionally, our results suggest that vaccines based on
620 *Pf*AMA1 may need to be designed to specifically avoid the effect of *Pf*MSP2 modulating
621 inhibitory antibodies, such as focussing on specific epitopes or structural features. To date,
622 vaccines based on AMA1 have failed to achieve substantial efficacy (Sagara et al., 2009;
623 Sheehy et al., 2012; Thera et al., 2011). We can speculate that one possible protective
624 mechanism of action of the Combination B vaccine (Genton et al., 2002; McCarthy et al.,
625 2011), which combined *Pf*MSP2, *Pf*MSP1 and *Pf*RESA, could be that the inhibitory activity
626 of vaccine-induced antibodies raised against *Pf*MSP2 were then able to potentiate the activity
627 of antibodies targeting other antigens, potentially *Pf*MSP1 which was also a target of the
628 vaccine. Further investigation using the parasite lines developed in this study and a wider panel
629 of antibodies could shed more light on this potentially novel mechanism of vaccine derived
630 antibody efficacy.

631 The results of this study and work done by Escalante et al. (2022) demonstrate that MSP2-like
632 sequences are found in the avian malarias *P. galinaceum* and *P. relictum*, which differs from
633 the fields previous understanding that *Pf*MSP2 arose in the *Laverania* lineage of malaria
634 parasites. This observation indicates that MSP2 was likely present in the ancestral malaria
635 parasite before being lost in primate and rodent *Plasmodium* spp. Further insights into the
636 evolution and loss of *Pf*MSP2 are likely to be found with additional whole genome sequences
637 of bird and lizard malaria species. The presence of *msp2*-like sequences in some avian
638 *Plasmodium* species and *Laverania* suggest a retention of *msp2* sequences in the *Laverania*
639 which indicates an important role for MSP2 for these parasites. Indeed, our amino acid and
640 structural prediction level comparison demonstrates that much of the protein properties
641 conserved in the *Laverania* MSP2s are also recognisable, and in many cases conserved, in the
642 avian malaria MSP2s, despite 10 million years of evolutionary divergence. This suggests that
643 having an MSP2-like protein is beneficial for these parasites with very different hosts.
644 However, CRISPR-Cas9 gene editing used in this work has shown that, in contrast to previous
645 work, *Pf*MSP2 is not essential for *P. falciparum* blood stage parasite growth *in vitro*. Our
646 findings raise the possibility that the retention of *Pf*MSP2 in the *Laverania*, and by association
647 potentially the avian malaria parasites, may be linked to its apparent capacity to modulate the
648 impact of antibodies against other merozoite surface-exposed antigens, rather than through a

649 direct mechanistic role in host-cell invasion. If MSP2 was to fulfill such a role in the *Laverania*
650 and avian malaria parasites, it raises the question of whether a similar protective system exists
651 in other *Plasmodium* spp. and what the key protein/s are that fulfil this role in these parasites.

652 The *Pf*3D7 MSP2 and *Pf*Dd2 MSP2 lines developed in this study will provide useful reagents
653 for investigating the potential of targeting a single, or both, *Pf*MSP2 allelic types with vaccines
654 that elicit different immune responses. These parasites could also be used to explore whether
655 vaccine-induced antibodies against other merozoite antigens could also be potentiated if any
656 immune evasion mechanism provided by *Pf*MSP2 is removed. This may be achievable with a
657 combination vaccine or through targeting an epitope of another merozoite vaccine candidate
658 that is not protected by *Pf*MSP2. Such information, investigated using the *Pf*MSP2 knock-out
659 parasites developed in this study, could be useful in prioritising vaccine candidates, specific
660 epitopes and combinations that target the merozoite.

661 **Conclusion**

662 Advancements in gene-editing techniques in *P. falciparum* have allowed us to show for the
663 first time, and contrary to previous work, that *Pf*MSP2 is not essential for *P. falciparum* growth
664 *in vitro*. Instead, we present a new concept that MSP2 can modulate the activity of invasion-
665 inhibitory antibodies and may have evolved for this purpose. It is possible that other merozoite
666 surface proteins may have similar roles and should be investigated in future studies. Our
667 observation that loss of *Pf*MSP2 potentiates the inhibitory activity of antibodies targeting other
668 merozoite surface exposed proteins reveals a new avenue to explore in vaccine development
669 by blocking or bypassing this function to improve the activity of vaccines targeting these
670 antigens.

671

672 **Materials and Methods**

673

674 **Bioinformatic analysis of *Pf*MSP2, *Pf*MSP4 and *Pf*MSP5 like proteins in *Plasmodium* spp.**

675 The PlasmoDB database (Aurrecoechea et al., 2009) was used to identify in the available
676 *Plasmodium* genomes the region between Adenylosuccinate lyase (PF3D7_0206700) and a
677 conserved protein of unknown function (PF3D7_0207100) where *Pf*MSP2, *Pf*MSP4 and
678 *Pf*MSP5 are localised in *P. falciparum*. All annotated MSP2, MSP4 and MSP5 protein
679 sequences were downloaded. Translated sequences of unannotated genes and putative

680 annotations in this region were also downloaded and aligned using the MUSCLE alignment
681 tool MEGA11: Molecular Evolutionary Genetics Analysis version 11 (Tamura et al., 2021) or
682 the Geneious Prime 2019.2.1 MUSCLE alignment tool (Biomatters Ltd.) and determined to be
683 MSP2, MSP4 or MSP5 based on sequence similarity in the conserved regions of these genes.
684 A BLAST (NCBI) search with the N-terminal and C-terminal conserved regions of MSP2 was
685 also performed to capture any sequences missed by the above approach. A maximum likelihood
686 phylogenetic tree of identified MSP2 sequences was generated using the default maximum
687 likelihood settings of MEGA11 with 500 bootstraps and the *P. gallinaceum* MSP2 as an
688 outgroup.

689

690 **Modelling of MSP structure across Plasmodium spp. using Alpha-fold**

691 In order to obtain models of the 3-dimensional protein structures of MSP2 for *P. falciparum*,
692 *P. reichenowi*, *P. billcollinsi*, *P. adleri*, *P. relictum* and *P. gallinaceum*, we first removed the
693 predicted N-terminal signal sequences and C-terminal GPI anchor sequence. The resulting
694 sequences were submitted to AlphaFold2 (Jumper et al., 2021). The resulting models were
695 subsequently analysed and visualised using PyMOL 2.4.0 (Schrödinger, USA).

696

697 **Culture and synchronisation of *P. falciparum***

698 *Plasmodium falciparum* 3D7 and Dd2 was cultured in RPMI-HEPES media (Gibco) containing
699 0.5% Albumax ll (Gibco), 25 µM Gentamicin (Gibco), 367 µM hypoxanthine (Sigma Aldrich),
700 2 mM L-Glutamax (Gibco), 0.17% sodium bicarbonate (Sigma Aldrich) and O positive human
701 red blood cells (Lifeblood, Australia) at 3% parasitemia, 3% haematocrit. Cultures were grown
702 at 37°C under 1% oxygen, 5% CO_2 (BOC gas), in a humidified chamber. For gene-edited lines,
703 WR99210 (Jakobus Pharmaceuticals) was added to culture media. Sorbitol lysis (5%) (Sigma
704 Aldrich) to select for ring-stage parasites, Percoll Plus (Sigma Aldrich) selection of late-stage
705 parasites and heparin treatment (Pfizer) (Boyle et al., 2010b) were used to maintain
706 synchronicity of parasite cultures.

707

708 **Generation of *Pf*MSP2 knockout line using CRISPR Cas9**

709 Briefly, a flank region incorporating the 5' region upstream of *Pf*MSP2, the first 44 amino
710 acids of the protein, and a flank of the region immediately 3' of *Pf*MSP2 was inserted into the

711 pCC1 plasmid by restriction enzyme cloning. A 20 bp guide sequence was designed using
712 EuPaGDT (Peng and Tarleton, 2015), annealed and inserted in the pUF_Cas9 plasmid by
713 infusion cloning (Takara Bio). pUF_Cas9 guide plasmid (20 μg) and pCC1 *Pf*MSP2 repair
714 plasmid (60 μg) was transfected directly into *P. falciparum* schizonts. Early schizonts were
715 purified using a 70% percoll gradient and treated for 4 hrs with compound 1 (Taylor et al.,
716 2010) at 2 μM. After incubation treated schizonts were washed twice and left shaking for 20
717 minutes before pelleting and resuspension in Complete Cytomix (plasmids plus 0.895% KCl,
718 0.0017% $CaCl_2$, 0.076% EGTA, 0.102% $MgCl_2$, 0.0871% K_2HPO_4, 0.068% KH_2PO_4, 0.708%
719 HEPES). Schizonts were electroporated in 0.2 cm cuvettes (Biorad) at 800 V and 25 μF.
720 Electroporated schizonts were mixed with warmed media and fresh RBCs and shaken to
721 promote invasion for 20 minutes after which they were placed in a culture dish. Transfected
722 parasites were then treated with WR99210 to select for integration of the hDHFR drug selection
723 cassette and MSP2 knock-out.

724 To confirm integration gDNA was collected by saponin lysis of schizont stage parasite culture
725 and gDNA extracted using the PureLink Genomic DNA Mini Kit (Invitrogen) as per
726 manufacturer's instructions. Integration of the *Pf*MSP2 knockout construct into a portion of
727 parasites was confirmed by PCR (Supplementary Table 1). Once confirmed cultures were
728 cycled on and off WR99210 (Jakobus Pharmaceuticals) and 1 μM 5FC (Sigma Aldrich) to
729 select for integrated parasites no longer expressing the guide plasmid. Limited dilution cloning
730 was then performed to obtain parasite clones which had integrated the knockout construct.

731

732 **Western blotting to detect *Pf*MSP2**

733 Synchronised schizonts were harvested and the RBCs lysed by saponin. Briefly ~10 mL
734 schizont (38-44 hrs) culture was lysed on ice for 10 minutes with 0.15% w/v saponin before
735 pelleting by centrifugation and washing once in 0.075% w/v saponin followed by three washes
736 in PBS containing protease inhibitors (CØmplete, Roche). Saponin treated schizont pellets
737 were treated with DNAsel (Qiagen) for 10 minutes at room temperature before resuspension
738 in reducing sample buffer (0.125 M Tris-HCL, 4% SDS, 20% glycerol, 10% beta-
739 mercaptoethanol and 0.002% bromophenol blue). Proteins were separated by size using SDS-
740 PAGE 4-12% Bis-Tris Gels (Bolt, Invitrogen) at 110V for 80 minutes before transfer to a
741 nitrocellulose membrane (iBlot, Invitrogen) at 20V for 7 minutes. Blots were blocked from 1
742 hr to overnight in 3% skim milk PBS (Sigma Aldrich) before incubation with primary

743 antibodies (1/75000 mouse 2F2 anti-*Pf*MSP2 3D7 (Supplementary Table 2; (Adda et al.,
744 2012)) and 1/75000 rabbit anti-*Plasmodium* aldolase (Abcam) or 1/75000 rabbit anti-FC27 and
745 1/10000 mouse anti- EXP2 (a gift of Paul Gilson, Burnet Institute, Melbourne) for 1- 2 hrs.
746 IRDye 800CW goat anti-mouse (1/4000, LI-COR Biosciences) or IRDye 680RD goat anti-
747 rabbit (1/4000, LI-COR Biosciences) secondary antibodies were used for detection on the
748 Odyssey Infrared imaging system (LI-COR Biosciences). Quantification was performed using
749 Image Studio Lite 5.2.5 (LI-COR Biosciences).

750 **Quantification of parasite expansion rate and invasion inhibition**

751 Potential growth defects resulting from gene editing was assessed by flow cytometry. The
752 initial parasitemia of cultures was determined by flow cytometry and then measured again after
753 either 48 hrs or 96 hrs of growth. To determine parasitemia by flow cytometry Ethidium
754 Bromide (10 µg/mL BioRad) was added to 50 µL of 1% haematocrit culture for 30 mins to
755 allow for staining of parasite DNA. The stain was washed off and wells resuspended in 200µL
756 of PBS. Data was collected on a BD Accuri C6 Plus Flow Cytometer (BD Biosciences) and
757 analysed on FlowJo (FlowJo LLC). Briefly, forward scatter and side scatter was used to
758 determine the RBC population. From this population infected RBCs were gated on as highly
759 fluorescent in the PE channel. Final parasitemia was compared back to initial parasitemia to
760 determine the fold increase in parasitemia for each line.

761 To examine the invasion inhibitory effect of antibodies (Supplementary Table 2), 5 µL of
762 potential inhibitor was mixed with 45 µL of 0.2% schizont parasitemia at 1% haematocrit for
763 96 hrs before end parasitemia was determined by flow cytometry. Data is displayed as %
764 Growth of media only controls for each line.

765 To examine differences in RBC receptor preference RBCs were treated with different enzymes
766 that cleave different residues of RBC receptors which is used as a marker for which RBC
767 receptor/s are preferred by *P. falciparum* (Duraisingh et al., 2003). Infected RBCs at 1% ring
768 stage parasitemia were washed three times in RPMI-HEPES to remove excess protein. Packed
769 RBCs (20 µL) at 1% parasitemia were then resuspended with 5X RBC volume of pre-warmed
770 enzymes at desired concentration (Supplementary Table 3). RBC-enzyme mix was incubated
771 at 37°C for 45 mins with rotation to keep RBCs resuspended. Following incubation, RBCs
772 were washed three times and added to fresh complete media at 1% haematocrit in a U- bottom
773 96 well plate in technical duplicate. Plates were incubated for 72 hrs, sufficient time for *P.*
774 *falciparum* to complete one full cycle of growth and reach trophozoite stage again. Final

775 parasitemia was determined by flow cytometry, as detailed above, and compared to non-treated
776 controls. IC_{50} calculations data was log transformed then a nonliner regression log-(inhibitor)-
777 versus-response curve was calculated with Extra Sum-of-Squares F Test (best-fit $LogIC_{50}$)
778 used to compared IC_{50}s between conditions.

779

780 **Immunofluorescence assay of Wildtype and *Pf*MSP2 KO parasites**

781 Schizonts ~38 hrs old were treated with E64 (Sigma-Aldrich) for 5 hrs to allow development
782 of very mature schizonts desired for imaging. After E64 treatment, parasite cultures were fixed
783 in 4% v/v paraformaledehyde (PFA, Sigma-Aldrich), 0.0075% v/v glutaraldehyde (pH 7.5,
784 Electron Microscopy Sciences) solution for 30 min at room temperature shaking gently. Fixed
785 parasites were washed in 1X PBS and then resuspended in PBS at 1% haematocrit. Coverslips
786 (#1.5H high-precision coverslips, Carl Zeiss, Oberkochen, Germany) were coated in 0.01%
787 Poly-L-lysine (Sigma Aldrich) for 1 hr at room temperature, washed in miliQ water before the
788 fixed parasite culture was allowed to adhere for 1 hr. Cells were permeabilised by 0.1% Triton
789 X-100 PBS for 10 mins before blocking for 1 hr to overnight in 3% BSA 0.05% Tween 20
790 PBS. Primary antibodies were diluted in 1% BSA 0.05% Tween 20 PBS and incubated for 2
791 hrs. Coverslips were washed in 0.05% Tween 20 PBS three times before incubation with the
792 secondary antibody (1/500 goat anti-chicken/mouse/rabbit Alexa Fluor coupled secondary
793 antibodies -488 nm, 594 nm, 647 nm; Life Technologies) for 1 hr. After the secondary antibody
794 was washed off coverslips underwent a secondary fix in 4% v/v PFA, 0.0075% v/v
795 glutaraldehyde for 5 mins. The fixative was washed off and the coverslips dehydrated with
796 sequential 3 min ethanol treatment (70%, 90% and 100%). Coverslips were allowed to dry and
797 mounted with ProLong Gold antifade solution (refractive index 1.4) which contains 4', 6-
798 diamidino-2phenylindole, dihydrochloride (DAPI) (ThermoFisher Scientific) and allowed to
799 set overnight. Imaging was performed on the Zeiss LSM 800 using the Airyscan super-
800 resolution mode (Carl Zeiss, Obekochen, Germany).

801

802 **Live cell microscopic analysis of merozoite RBC invasion**

803 Highly synchronised *Pf*Dd2 and *Pf*Dd2 ΔMSP2 parasites at schizont stages were adjusted to
804 0.25% Haematocrit in complete culture medium. A volume of 200 μL was added to a well of
805 an iBidi 15 μ-Slide 8 well, glass bottom slide (iBidi 80827) and the slide was promptly returned
806 to sit on a prewarmed water block within a gassed box and left to incubate at 37ºC to allow

807 iRBCs to settle. The slide was then transported directly to a prewarmed Nikon TiE microscope
808 with an environmental chamber heated to 37°C and gas mixture of 1% O_2, 5% CO_2 and 94%
809 nitrogen. Filming was conducted using either a 60X water or 100X oil objective. Differential
810 interference contrast (DIC) imaging was captured at 3 – 3.5 Volts with a camera exposure of
811 60 – 180 milliseconds.

812 Captured footage was processed using the Nikon analysis software (NIS-Elements AR
813 Analysis version 5.21.01) and analysis of the schizont rupture and merozoite invasion events
814 was performed manually. The merozoites which invaded successfully were tracked and
815 attachment time, reorientation time (if obvious), deformation start and end times, the
816 deformation score (Weiss et al., 2015; Wilson et al., 2015), invasion initiation and completion
817 times and echinocytosis start times were recorded.

818

819 **RNA extraction**

820 Highly synchronised cultures were pelleted, resuspended in TriZol (Invitrogen) and incubated
821 for 5 minutes at 37°C. Chloroform (Sigma Aldrich) was added, mixed and then spun at 12,000g
822 for 30 minutes at 4°C. Supernatant was collected and mixed with an equal volume of 70%
823 Ethanol and processed using the RNeasy Kit (Qiagen) to extract purified RNA. RNA was
824 DNAse l (Qiagen) treated for 30 mins at room temperature and cleaned up on RNeasy columns
825 according to the manufacturers protocol. Absence of gDNA was checked by qPCR of gDNA
826 with primers (*Pf*SUB1) and DNAse I treatment repeated if necessary.

827

828 **qPCR of gene expression in schizonts**

829 DNAse treated RNA was added to 40 mM dNTPs (Qiagen), 0.4 mg/mL random hexamer
830 (Qiagen) and incubated at 65°C for 5 mins. After incubation 5x Superscript Buffer (Invitrogen),
831 100 mM DTT (Invitrogen), 40 U/µL RNAseOUT (Invitrogen) and 200 µ/mL Superscript lll
832 Reverse Transcriptase (Invitrogen) was added and cycled 25°C 5 mins, 50°C for 60 mins and
833 70°C for 15 mins. Primers (Supplementary Table 4) were designed to detect *Pf*MSP2, *Pf*MSP4,
834 *Pf*MSP5, *Pf*SUB1 and Fructose Bisphosphate Aldolase as a reference gene (Salanti et al.,
835 2003). qPCR was performed on cDNA from WT and knockout parasites with PowerUp SYBR
836 Green Master Mix (Applied Biosystems) and cycling parameters; 95°C for 10 mins followed
837 by 40 cycles 95°C for 15 mins, 60°C for 14 mins before a dissociation step at 95°C for 2 mins

838 followed by 60ºC for 2 mins with a 2% ramp to 95ºC for 2 mins on the QuantStudio 7 Flex
839 System (ThermoFisher). qPCR was performed in triplicate for each of the three independent
840 experiments. Change in gene expression in knockout lines compared to WT was quantified by
841 the $2^{-\Delta\Delta Ct}$ method (Livak and Schmittgen, 2001).

842

843 **Differential gene expression in *Pf*MSP2 KO compared to WT schizonts**

844 RNA sequencing of the schizont stage transcriptome of *Pf*3D7 MSP2 KO and *Pf*3D7 WT was
845 performed using the Illumina total RNA with Ribo Zero plus for library preparation and
846 sequenced on the NovaSeq 6000 platform with 2x150 bp paired end reads (Supplementary
847 Table 5). Reads were aligned to the *Pf*3D7 reference genome (PlasmoDB v61) using STAR
848 aligner (Dobin et al., 2013). Reads were called using Rsubread FeatureCounts (Liao et al.,
849 2014) with reads counted by CDS and summarised by gene. Differential gene analysis was
850 performed with DESeq2 (Love et al., 2014) and visualized in R studio using ggplots2
851 (Wickham, 2016).

852

853 **Quantitative Immunofluorescence assay**

854 Synchronous *Pf*3D7 MSP2 KO and *Pf*3D7 WT parasite cultures were treated with ML10
855 (Ressurreição et al., 2020) to allow mature schizonts to develop. Thin blood smears were then
856 made and fixed in 100%, -20°C methanol for 5 mins. Blocking of smears was performed in 1%
857 BSA PBS, then fluorophore conjugated WD34 (240 ng/mL) and WD33 (120 ng/mL) i-bodies
858 (Angage et al., 2024) in 1% BSA PBS were added and incubated at room temperature for 1 hr.
859 Smears were then washed, ethanol dehydrated and a coverslip mounted (ProLong Diamond
860 Antifade mountant with DAPI (refractive index 1.47, ThermoFisher Scientific)) and allowed
861 to cure for 48 hrs at room temperature. Fluorescence images were acquired using an Olympus
862 FV3000 confocal microscope equipped with a 100x oil objective (NA 1.4). Quantification of
863 parasite associated fluorescence was performed using a modified image analysis pipeline
864 (Liffner et al., 2020) implemented in Imaris™ (9.9 version) where non-specific background
865 fluorescence was removed using rolling ball background subtraction and a thresholding
866 algorithm applied to the image to generate binary masks, separating objects exceeding the
867 threshold (putative parasites) from the background. Binary masks were further refined to
868 exclude objects smaller or larger than a defined size range (< 3 μm and > 15 μm),
869 corresponding to the expected size of AMA i-body stained schizonts. Following segmentation

870 the surface area containing antibody signal were calculated and these values compared between
871 *Pf*3D7 MSP2 KO and *Pf*3D7 WT parasites.
872

873 **Surface Plasmon Resonance (SPR) Assay**

874 Surface plasmon resonance (SPR) was employed to determine the association rate constant
875 (K_a) of AMA1-antibody interactions in the presence of MSP2 using the Biacore T200 system
876 (Cytiva). Flow cells 1, 2, and 3 were activated for 14 minutes using a 1:1 mixture of 0.1 M N-
877 hydroxysuccinimide (NHS) and 0.4 M N-(3-dimethylaminopropyl)-N'-ethylcarbodiimide
878 hydrochloride (EDC) at a flow rate of 5 µL/min. Flow cell one was immobilised with bovine
879 serum albumin (BSA) to serve as a reference surface. AMA1 was immobilised at a
880 concentration of 80 µg/mL in 10 mM sodium acetate (pH 4.5) to achieve a surface density of
881 1000 response units (RU) on flow cells Two and three. MSP2 was co-immobilised in flow
882 cell three to a surface density of 2000 RU. All surfaces were subsequently blocked with a 7-
883 minute injection of 1 M ethanolamine (pH 8.0). Purified antibodies were prepared in PBS
884 containing 0.005% Tween-20 (pH 7.4) and injected over the flow cells at a flow rate of 60
885 µL/min at 25°C. Single-cycle kinetics, using a bivalent analyte model, was applied to analyse
886 the interactions.

887

888 **Enzyme-Linked Immunosorbent Assay (ELISA)**

889 ELISAs to evaluate the effect of MSP2 on the binding of AMA1-specific antibodies were
890 carried out in a volume of 100 µL per well, either at room temperature for 1 hr or overnight
891 at 4°C. All washing steps consisted of three washes with PBS containing 0.1% Tween-20
892 (PBS-T). Nunc Maxisorp plates (Thermo Fisher Scientific, USA) were coated with AMA1
893 at a concentration of 0.8 µg/mL, followed by washing and subsequent coating with
894 increasing concentrations of MSP2. Wells were then blocked with 5% (w/v) skim milk in
895 PBS and then incubated for 1 hr at room temperature with the anti-AMA1 antibodies mouse
896 Fc-conjugated WD34 i-body or mouse monoclonal antibody (mAb) 4G2, or with anti-MSP2
897 mAb 9D8, at a concentration of 2.5 µg/mL. The primary antibody was washed off and the
898 HRP-conjugated secondary antibody (1:5000, Sigma Aldrich) was then applied for 1 hr at
899 room temperature before washing. For signal development to detect bound primary
900 antibodies, wells were incubated with 1-Step™ Ultra TMB-ELISA Substrate Solution
901 (Thermo Fisher Scientific, USA) according to the manufacturers instructions. The reaction

902 was stopped by adding 1 M sulfuric acid, and the absorbance at 450 nm was measured using
903 a microplate reader.

904

905 **Statistical Analysis**

906 Three independent experiments were performed for all experiments in technical duplicate,
907 unless otherwise stated. Data was graphed and statistical tests performed in Prism GraphPad
908 v9 or R.

909

910

911 **Acknowledgements**

912 The authors would like to thank Alan Cowman, Stephen Scally and Jennifer Thompson
913 (WEHI, Melbourne) for provision of PCRCR complex antibodies, Paul Gilson (Burnet
914 Institute, Melb) for EXP2 antibodies, Dr Chris MacRaild (Monash University) for helpful
915 discussion, Dr Sonja Frölich (the University of Adelaide) for assistance on quantitative
916 immunofluorescence assays and Adelaide Microscopy for training and use of microscopy
917 instruments. We thank Lifeblood, Australia, for provision of RBCs. DWW was supported by
918 a Hospital Research Foundation (C-MCF-52-2019) and Australian Research Council
919 (FT240100420) Future Fellowship. DWW and JGB by a Hospital Research Foundation
920 Collaborative Grant (S-03-EOI-2021). JGB was supported by the National Health and Medical
921 Research Council of Australia (Research Fellowship and Investigator Grant to JGB, Australian
922 Centre for Research Excellence in Malaria Research). IGH and JC were supported by an
923 Australian Research Council RTP scholarship. The Burnet Institute is supported by the
924 NHMRC for Independent Research Institutes Infrastructure Support Scheme and the Victorian
925 State Government Operational Infrastructure Support.

926

927 **Author Contributions**

928 Conceived and designed the experiments: DWW, IGH, JC, JGB, DA, MF, RA. Performed the
929 experiments and phylogenetic analysis: IGH, JC, KHL, OR, DA, KRT, NB. Analysed the data:
930 IGH, DWW, JC, KHL, OR, DA, MF. Provided key discussions on PfMSP2 and/or key
931 reagents: RA, MF, DA. Paper writing: DWW, JC, IGH, JGB with critical input from RA, MF,

932 DA, OR, KRT and based on the PhD thesis of IGH.

933

934 **Competing Interests**

935 M.F. is the founding chief scientist and a shareholder in AdAlta Ltd., and R.F.A. is also a
936 shareholder in AdAlta. The other authors have declared no competing interests.

937

938 **References**

939 Adda, C.G., MacRaild, C.A., Reiling, L., Wycherley, K., Boyle, M.J., Kienzle, V., Masendycz, P., Foley, M.,
940 Beeson, J.G., Norton, R.S., Anders, R.F., 2012. Antigenic characterization of an intrinsically
941 unstructured protein, Plasmodium falciparum merozoite surface protein 2. Infect Immun 80,
942 4177–4185. https://doi.org/10.1128/IAI.00665-12

943 Adda, C.G., Murphy, V.J., Sunde, M., Waddington, L.J., Schloegel, J., Talbo, G.H., Vingas, K., Kienzle, V.,
944 Masciantonio, R., Howlett, G.J., Hodder, A.N., Foley, M., Anders, R.F., 2009. Plasmodium
945 falciparum merozoite surface protein 2 is unstructured and forms amyloid-like fibrils. Mol
946 Biochem Parasitol 166, 159–171. https://doi.org/10.1016/j.molbiopara.2009.03.012

947 Alanine, D.G.W., Quinkert, D., Kumarasingha, R., Mehmood, S., Donnellan, F.R., Minkah, N.K.,
948 Dadonaite, B., Diouf, A., Galaway, F., Silk, S.E., Jamwal, A., Marshall, J.M., Miura, K., Foquet, L.,
949 Elias, S.C., Labbé, G.M., Douglas, A.D., Jin, J., Payne, R.O., Illingworth, J.J., Pattinson, D.J., Pulido,
950 D., Williams, B.G., de Jongh, W.A., Wright, G.J., Kappe, S.H.I., Robinson, C. V, Long, C.A., Crabb,
951 B.S., Gilson, P.R., Higgins, M.K., Draper, S.J., 2019. Human Antibodies that Slow Erythrocyte
952 Invasion Potentiate Malaria-Neutralizing Antibodies. Cell 178, 216-228.e21.
953 https://doi.org/10.1016/j.cell.2019.05.025

954 Anders, R.F., Adda, C.G., Foley, M., Norton, R.S., 2010. Recombinant protein vaccines against the
955 asexual blood-stages of Plasmodium falciparum. Hum Vaccin 6, 39–53.
956 https://doi.org/10.4161/hv.6.1.10712

957 Angage, D., Chmielewski, J., Maddumage, J.C., Hesping, E., Caiazzo, S., Lai, K.H., Yeoh, L.M., Menassa,
958 J., Opi, D.H., Cairns, C., Puthalakath, H., Beeson, J.G., Kvansakul, M., Boddey, J.A., Wilson, D.W.,
959 Anders, R.F., Foley, M., 2024. A broadly cross-reactive i-body to AMA1 potently inhibits blood
960 and liver stages of Plasmodium parasites. Nat Commun 15, 7206.
961 https://doi.org/10.1038/s41467-024-50770-7

962 Aurrecoechea, C., Brestelli, J., Brunk, B.P., Dommer, J., Fischer, S., Gajria, B., Gao, X., Gingle, A., Grant,
963 G., Harb, O.S., Heiges, M., Innamorato, F., Iodice, J., Kissinger, J.C., Kraemer, E., Li, W., Miller, J.A.,
964 Nayak, V., Pennington, C., Pinney, D.F., Roos, D.S., Ross, C., Stoeckert, J.C.J., Treatman, C., Wang,
965 H., 2009. PlasmoDB: a functional genomic database for malaria parasites. Nucleic Acids Res 37,
966 D539–D543. https://doi.org/10.1093/nar/gkn814

967 Bannister, L.H., Mitchell, G.H., Butcher, G.A., Gennis, E.D., Cohen, S., 1986. Structure and development
968 of the surface coat of erythrocytic merozoites of Plasmodium knowlesi. Cell Tissue Res 245, 281–
969 290.

970 Baum, J., Maier, A.G., Good, R.T., Simpson, K.M., Cowman, A.F., 2005. Invasion by P. falciparum
971 Merozoites Suggests a Hierarchy of Molecular Interactions. PLoS Pathog 1, e37.

972 Beeson, J.G., Drew, D.R., Boyle, M.J., Feng, G., Fowkes, F.J.I.I., Richards, J.S., 2016. Merozoite surface
973 proteins in red blood cell invasion, immunity and vaccines against malaria. FEMS Microbiol Rev
974 40, 343–372. https://doi.org/10.1093/femsre/fuw001

975 Beeson, J.G., Kurtovic, L., Dobaño, C., Opi, D.H., Chan, J.-A., Feng, G., Good, M.F., Reiling, L., Boyle,
976 M.J., 2019. Challenges and strategies for developing efficacious and long-lasting
977 malaria vaccines. Sci Transl Med 11. https://doi.org/10.1126/scitranslmed.aau1458

978 Black, C.G., Barnwell, J.W., Huber, C.S., Galinski, M.R., Coppel, R.L., 2002. The Plasmodium vivax
979 homologues of merozoite surface proteins 4 and 5 from Plasmodium falciparum are expressed
980 at different locations in the merozoite. Mol Biochem Parasitol 120, 215–224.
981 https://doi.org/https://doi.org/10.1016/S0166-6851(01)00458-3

982 Böhme, U., Otto, T.D., Cotton, J.A., Steinbiss, S., Sanders, M., Oyola, S.O., Nicot, A., Gandon, S., Patra,
983 K.P., Herd, C., Bushell, E., Modrzynska, K.K., Billker, O., Vinetz, J.M., Rivero, A., Newbold, C.I.,
984 Berriman, M., 2018. Complete avian malaria parasite genomes reveal features associated with
985 lineage-specific evolution in birds and mammals. Genome Res 28, 547–560.
986 https://doi.org/10.1101/gr.218123.116

987 Boyle, M.J., Langer, C., Chan, J.-A., Hodder, A.N., Coppel, R.L., Anders, R.F., Beeson, J.G., 2014.
988 Sequential Processing of Merozoite Surface Proteins during and after Erythrocyte Invasion by
989 Plasmodium falciparum. Infect Immun 82, 924–936. https://doi.org/10.1128/IAI.00866-13

990 Boyle, M.J., Reiling, L., Feng, G., Langer, C., Osier, F.H., Aspeling-Jones, H., Cheng, Y.S., Stubbs, J.,
991 Tetteh, K.K.A., Conway, D.J., McCarthy, J.S., Muller, I., Marsh, K., Anders, R.F., Beeson, J.G., 2015.
992 Human antibodies fix complement to inhibit plasmodium falciparum invasion of erythrocytes

993 and are associated with protection against malaria. Immunity 42, 580–590.
994 https://doi.org/10.1016/j.immuni.2015.02.012

995 Boyle, M.J., Richards, J.S., Gilson, P.R., Chai, W., Beeson, J.G., 2010a. Interactions with heparin-like
996 molecules during erythrocyte invasion by Plasmodium falciparum merozoites. Blood 115, 4559–
997 4568. https://doi.org/10.1182/blood-2009-09-243725

998 Boyle, M.J., Wilson, D.W., Richards, J.S., Riglar, D.T., Tetteh, K.K.A., Conway, D.J., Ralph, S.A., Baum, J.,
999 Beeson, J.G., 2010b. Isolation of viable Plasmodium falciparum merozoites to define erythrocyte
1000 invasion events and advance vaccine and drug development. Proc Natl Acad Sci U S A 107,
1001 14378–14383. https://doi.org/10.1073/pnas.1009198107

1002 Coley, A.M., Gupta, A., Murphy, V.J., Bai, T., Kim, H., Anders, R.F., Foley, M., Batchelor, A.H., 2007.
1003 Structure of the Malaria Antigen AMA1 in Complex with a Growth-Inhibitory Antibody. PLoS
1004 Pathog 3, e138.

1005 Cowman, A.F., Tonkin, C.J., Tham, W.-H., Duraisingh, M.T., 2017. The Molecular Basis of Erythrocyte
1006 Invasion by Malaria Parasites. Cell Host Microbe 22, 232–245.
1007 https://doi.org/10.1016/j.chom.2017.07.003

1008 Crosnier, C., Bustamante, L.Y., Bartholdson, S.J., Bei, A.K., Theron, M., Uchikawa, M., Mboup, S., Ndir,
1009 O., Kwiatkowski, D.P., Duraisingh, M.T., Rayner, J.C., Wright, G.J., 2011. Basigin is a receptor
1010 essential for erythrocyte invasion by Plasmodium falciparum. Nature 480, 534–537.
1011 https://doi.org/10.1038/nature10606

1012 Das, S., Hertrich, N., Perrin, A.J., Withers-Martinez, C., Collins, C.R., Jones, M.L., Watermeyer, J.M.,
1013 Fobes, E.T., Martin, S.R., Saibil, H.R., Wright, G.J., Treeck, M., Epp, C., Blackman, M.J., 2015.
1014 Processing of Plasmodium falciparum Merozoite Surface Protein MSP1 Activates a Spectrin-
1015 Binding Function Enabling Parasite Egress from RBCs. Cell Host Microbe 18, 433–444.
1016 https://doi.org/10.1016/j.chom.2015.09.007

1017 Datoo, M.S., Dicko, A., Tinto, H., Ouédraogo, J.B., Hamaluba, M., Olotu, A., Beaumont, E., Ramos
1018 Lopez, F., Natama, H.M., Weston, S., Chemba, M., Compaore, Y.D., Issiaka, D., Salou, D., Some,
1019 A.M., Omenda, S., Lawrie, A., Bejon, P., Rao, H., Chandramohan, D., Roberts, R., Bharati, S.,
1020 Stockdale, L., Gairola, S., Greenwood, B.M., Ewer, K.J., Bradley, J., Kulkarni, P.S., Shaligram, U.,
1021 Hill, A.V.S., Mahamar, A., Sanogo, K., Sidibe, Y., Diarra, K., Samassekou, M., Attaher, O., Tapily,
1022 A., Diallo, M., Dicko, O.M., Kaya, M., Maguiraga, S.O., Sankare, Y., Yalcouye, H., Diarra, S.,
1023 Niambele, S.M., Thera, I., Sagara, I., Sylla, M., Dolo, A., Misidai, N., Simando, S., Msami, H., Juma,
1024 O., Gutapaka, N., Paul, R., Mswata, S., Sasamalo, I., Johaness, K., Sultan, M., Alexander, A.,

1025 Kimaro, I., Lwanga, K., Mtungwe, M., Khamis, K., Rugarabam, L., Kalinga, W., Mohammed, M.,
1026 Kamange, J., Msangi, J., Mwaijande, B., Mtaka, I., Mhapa, M., Mlaganile, T., Mbaga, T., Yerbanga,
1027 R.S., Samtouma, W., Sienou, A.A., Kabre, Z., Ouedraogo, W.J.M., Yarbanga, G.A.B., Zongo, I.,
1028 Savadogo, H., Sanon, J., Compaore, J., Kere, I., Yoni, F.L., Sanre, T.M., Ouattara, S.B., Provstgaard-
1029 Morys, S., Woods, D., Snow, R.W., Amek, N., Ngetsa, C.J., Ochola-Oyier, L.I., Musyoki, J., Munene,
1030 M., Mumba, N., Adetifa, U.J., Muiruri, C.M., Mwawaka, J.S., Mwaganyuma, M.H., Ndichu, M.N.,
1031 Weya, J.O., Njogu, K., Grant, J., Webster, J., Lakhkar, A., Ido, N.F.A., Traore, O., Tahita, M.C.,
1032 Bonko, M. dit A., Rouamba, T., Ouedraogo, D.F., Soma, R., Millogo, A., Ouedraogo, E., Sorgho, F.,
1033 Konate, F., Valea, I., 2024. Safety and efficacy of malaria vaccine candidate R21/Matrix-M in
1034 African children: a multicentre, double-blind, randomised, phase 3 trial. The Lancet 403, 533–
1035 544. https://doi.org/10.1016/S0140-6736(23)02511-4

1036 Dobin, A., Davis, C.A., Schlesinger, F., Drenkow, J., Zaleski, C., Jha, S., Batut, P., Chaisson, M., Gingeras,
1037 T.R., 2013. STAR: ultrafast universal RNA-seq aligner. Bioinformatics 29, 15–21.
1038 https://doi.org/10.1093/bioinformatics/bts635

1039 Douglas, A.D., Williams, A.R., Illingworth, J.J., Kamuyu, G., Biswas, S., Goodman, A.L., Wyllie, D.H.,
1040 Crosnier, C., Miura, K., Wright, G.J., Long, C.A., Osier, F.H., Marsh, K., Turner, A. V., Hill, A.V.S.,
1041 Draper, S.J., 2011. The blood-stage malaria antigen PfRH5 is susceptible to vaccine-inducible
1042 cross-strain neutralizing antibody. Nat Commun 2, 601. https://doi.org/10.1038/ncomms1615

1043 Duraisingh, M.T., Maier, A.G., Triglia, T., Cowman, A.F., 2003. Erythrocyte-binding antigen 175
1044 mediates invasion in Plasmodium falciparum utilizing sialic acid-dependent and -independent
1045 pathways. Proc Natl Acad Sci U S A 100, 4796–4801. https://doi.org/10.1073/pnas.0730883100

1046 Eisenhaber, B., Bork, P., Eisenhaber, F., 1999. Prediction of potential GPI-modification sites in
1047 proprotein sequences. J Mol Biol 292, 741–58. https://doi.org/10.1006/jmbi.1999.3069

1048 Escalante, A.A., Cepeda, A.S., Pacheco, M.A., 2022. Why Plasmodium vivax and Plasmodium
1049 falciparum are so different? A tale of two clades and their species diversities. Malar J 21, 139.
1050 https://doi.org/10.1186/s12936-022-04130-9

1051 Feng, G., Boyle, M.J., Cross, N., Chan, J.-A., Reiling, L., Osier, F., Stanisic, D.I., Mueller, I., Anders, R.F.,
1052 McCarthy, J.S., Richards, J.S., Beeson, J.G., 2018. Human Immunization With a Polymorphic
1053 Malaria Vaccine Candidate Induced Antibodies to Conserved Epitopes That Promote Functional
1054 Antibodies to Multiple Parasite Strains. J Infect Dis 218, 35–43.
1055 https://doi.org/10.1093/infdis/jiy170

1056 Ferreira, E. d'Avila, Alexandre, M.A., Salinas, J.L., de Siqueira, A.M., Benzecry, S.G., de Lacerda, M.V.G.,
1057 Monteiro, W.M., 2015. Association between anthropometry-based nutritional status and
1058 malaria: a systematic review of observational studies. Malaria J 14, 346.
1059 https://doi.org/10.1186/s12936-015-0870-5

1060 Fowkes, F.J.I., Richards, J.S., Simpson, J.A., Beeson, J.G., 2010. The Relationship between Anti-
1061 merozoite Antibodies and Incidence of Plasmodium falciparum Malaria: A Systematic Review
1062 and Meta-analysis. PLoS Med 7, e1000218. https://doi.org/10.1371/journal.pmed.1000218

1063 Genton, B., Al-Yaman, F., Betuela, I., Anders, R.F., Saul, A., Baea, K., Mellombo, M., Taraika, J., Brown,
1064 G. V., Pye, D., Irving, D.O., Felger, I., Beck, H.-P.P., Smith, T.A., Alpers, M.P., 2003. Safety and
1065 immunogenicity of a three-component blood-stage malaria vaccine (MSP1, MSP2, RESA) against
1066 Plasmodium falciparum in Papua New Guinean children. Vaccine 22, 30–41.
1067 https://doi.org/https://doi.org/10.1016/S0264-410X(03)00536-X

1068 Genton, B., Betuela, I., Felger, I., Al-Yaman, F., Anders, R.F., Saul, A., Rare, L., Baisor, M., Lorry, K.,
1069 Brown, G. V, Pye, D., Irving, D.O., Smith, T.A., Beck, H.-P., Alpers, M.P., 2002. A Recombinant
1070 Blood-Stage Malaria Vaccine Reduces Plasmodium falciparum Density and Exerts Selective
1071 Pressure on Parasite Populations in a Phase 1-2b Trial in Papua New Guinea. J Infect Dis 185,
1072 820–827.

1073 Gilson, P.R., Nebl, T., Vukcevic, D., Moritz, R.L., Sargeant, T., Speed, T.P., Schofield, L., Crabb, B.S.,
1074 2006. Identification and Stoichiometry of Glycosylphosphatidylinositol-anchored Membrane
1075 Proteins of the Human Malaria Parasite *Plasmodium falciparum*. Molecular & Cellular
1076 Proteomics 5, 1286–1299. https://doi.org/10.1074/mcp.M600035-MCP200

1077 Griffiths, K., Dolezal, O., Cao, B., Nilsson, S.K., See, H.B., Pfleger, K.D.G., Roche, M., Gorry, P.R., Pow,
1078 A., Viduka, K., Lim, K., Lu, B.G.C., Chang, D.H.C., Murray-Rust, T., Kvansakul, M., Perugini, M.A.,
1079 Dogovski, C., Doerflinger, M., Zhang, Y., Parisi, K., Casey, J.L., Nuttall, S.D., Foley, M., 2016. i-
1080 bodies, Human Single Domain Antibodies That Antagonize Chemokine Receptor CXCR4. J Biol
1081 Chem 291, 12641–12657. https://doi.org/10.1074/jbc.M116.721050

1082 Griffiths, K., Habiel, D.M., Jaffar, J., Binder, U., Darby, W.G., Hosking, C.G., Skerra, A., Westall, G.P.,
1083 Hogaboam, C.M., Foley, M., 2018. Anti-fibrotic Effects of CXCR4-Targeting i-body AD-114 in
1084 Preclinical Models of Pulmonary Fibrosis. Sci Rep 8, 3212. https://doi.org/10.1038/s41598-018-
1085 20811-5

1086 Jumper, J., Evans, R., Pritzel, A., Green, T., Figurnov, M., Ronneberger, O., Tunyasuvunakool, K., Bates,
1087 R., Žídek, A., Potapenko, A., Bridgland, A., Meyer, C., Kohl, S.A.A., Ballard, A.J., Cowie, A., Romera-

1088 Paredes, B., Nikolov, S., Jain, R., Adler, J., Back, T., Petersen, S., Reiman, D., Clancy, E., Zielinski,
1089 M., Steinegger, M., Pacholska, M., Berghammer, T., Bodenstein, S., Silver, D., Vinyals, O., Senior,
1090 A.W., Kavukcuoglu, K., Kohli, P., Hassabis, D., 2021. Highly accurate protein structure prediction
1091 with AlphaFold. Nature 596, 583–589. https://doi.org/10.1038/s41586-021-03819-2

1092 Kals, E., Kals, M., Lees, R.A., Introini, V., Kemp, A., Silvester, E., Collins, C.R., Umrekar, T., Kotar, J.,
1093 Cicuta, P., Rayner, J.C., 2024. Application of optical tweezer technology reveals that PfEBA and
1094 PfRH ligands, not PfMSP1, play a central role in Plasmodium falciparum merozoite-erythrocyte
1095 attachment. PLoS Pathog 20, e1012041. https://doi.org/10.1371/journal.ppat.1012041

1096 Kocken, C.H., van der Wel, A.M., Dubbeld, M.A., Narum, D.L., van de Rijke, F.M., van Gemert, G.J., van
1097 der Linde, X., Bannister, L.H., Janse, C., Waters, A.P., Thomas, A.W., 1998. Precise timing of
1098 expression of a Plasmodium falciparum-derived transgene in Plasmodium berghei is a critical
1099 determinant of subsequent subcellular localization. J Biol Chem 273, 15119–15124.
1100 https://doi.org/10.1074/jbc.273.24.15119

1101 Lamarque, M., Besteiro, S., Papoin, J., Roques, M., Vulliez-Le Normand, B., Morlon-Guyot, J.,
1102 Dubremetz, J.-F., Fauquenoy, S., Tomavo, S., Faber, B.W., Kocken, C.H., Thomas, A.W., Boulanger,
1103 M.J., Bentley, G.A., Lebrun, M., 2011. The RON2-AMA1 Interaction is a Critical Step in Moving
1104 Junction-Dependent Invasion by Apicomplexan Parasites. PLoS Pathog 7, e1001276.

1105 Li, X., Chen, H., Oo, T.H., Daly, T.M., Bergman, L.W., Liu, S.-C., Chishti, A.H., Oh, S.S., 2004. A co-ligand
1106 complex anchors Plasmodium falciparum merozoites to the erythrocyte invasion receptor band
1107 3. J Biol Chem 279, 5765–5771. https://doi.org/10.1074/jbc.M308716200

1108 Li, Y., Yang, L., Yang, L.-Q., 2024. Effects of intrinsically disordered regions in gp120 underlying
1109 HIV neutralization phenotypes. Biochem Biophys Res Commun 709, 149830.
1110 https://doi.org/10.1016/j.bbrc.2024.149830

1111 Liao, Y., Smyth, G.K., Shi, W., 2014. featureCounts: an efficient general purpose program for assigning
1112 sequence reads to genomic features. Bioinformatics 30, 923–930.
1113 https://doi.org/10.1093/bioinformatics/btt656

1114 Liffner, B., Frölich, S., Heinemann, G.K., Liu, B., Ralph, S.A., Dixon, M.W.A., Gilberger, T.W., Wilson,
1115 D.W., 2020. PfCERLI1 is a conserved rhoptry associated protein essential for Plasmodium
1116 falciparum merozoite invasion of erythrocytes. Nat Commun 11.
1117 https://doi.org/10.1038/s41467-020-15127-w

1118 Livak, K.J., Schmittgen, T.D., 2001. Analysis of Relative Gene Expression Data Using Real-Time
1119 Quantitative PCR and the 2−ΔΔCT Method. Methods 25, 402–408.
1120 https://doi.org/https://doi.org/10.1006/meth.2001.1262

1121 Love, M.I., Huber, W., Anders, S., 2014. Moderated estimation of fold change and dispersion for RNA-
1122 seq data with DESeq2. Genome Biol 15, 550. https://doi.org/10.1186/s13059-014-0550-8

1123 Lu, C., Zheng, X., Zhang, W., Zhao, H., MacRaild, C.A., Norton, R.S., Zhuang, Y., Wang, J., Zhang, X.,
1124 2019. Interaction of merozoite surface protein 2 with lipid membranes. FEBS Lett 593, 288–295.
1125 https://doi.org/10.1002/1873-3468.13320

1126 MacRaild, C.A., Pedersen, M.Ø., Anders, R.F., Norton, R.S., 2012. Lipid interactions of the malaria
1127 antigen merozoite surface protein 2. Biochim Biophys Acta 1818, 2572–8.
1128 https://doi.org/10.1016/j.bbamem.2012.06.015

1129 MacRaild, C.A., Zachrdla, M., Andrew, D., Krishnarjuna, B., Nováček, J., Žídek, L., Sklenář, V., Richards,
1130 J.S., Beeson, J.G., Anders, R.F., Norton, R.S., 2015. Conformational dynamics and antigenicity in
1131 the disordered malaria antigen merozoite surface protein 2. PLoS One 10, e0119899.
1132 https://doi.org/10.1371/journal.pone.0119899

1133 McCarthy, J.S., Marjason, J., Elliott, S., Fahey, P., Bang, G., Malkin, E., Tierney, E., Aked-Hurditch, H.,
1134 Adda, C., Cross, N., Richards, J.S., Fowkes, F.J.I., Boyle, M.J., Long, C., Druilhe, P., Beeson, J.G.,
1135 Anders, R.F., 2011. A phase 1 trial of MSP2-C1, a blood-stage malaria vaccine containing 2
1136 isoforms of MSP2 formulated with montanide® ISA 720. PLoS One 6.
1137 https://doi.org/10.1371/journal.pone.0024413

1138 Ocampo, M., Urquiza, M., Guzmán, F., Rodriguez, L.E., Suarez, J., Curtidor, H., Rosas, J., Diaz, M.,
1139 Patarroyo, M.E., 2003. Two MSA 2 peptides that bind to human red blood cells are relevant to
1140 Plasmodium falciparum merozoite invasion. The Journal of Peptide Research 55, 216–223.
1141 https://doi.org/10.1034/j.1399-3011.2000.00174.x

1142 Orlandi, P.A., Klotz, F.W., Haynes, J.D., 1992. A malaria invasion receptor, the 175-kilodalton
1143 erythrocyte binding antigen of Plasmodium falciparum recognizes the terminal Neu5Ac (alpha 2-
1144 3) Gal-sequences of glycophorin A. J Cell Biol 116, 901–909.

1145 Osier, F.H., Feng, G., Boyle, M.J., Langer, C., Zhou, J., Richards, J.S., McCallum, F.J., Reiling, L.,
1146 Jaworowski, A., Anders, R.F., Marsh, K., Beeson, J.G., 2014. Opsonic phagocytosis of Plasmodium
1147 falciparum merozoites: mechanism in human immunity and a correlate of protection against
1148 malaria. BMC Med 12, 108. https://doi.org/10.1186/1741-7015-12-108

1149 Osier, F.H.A., Murungi, L.M., Fegan, G., Tuju, J., Tetteh, K.K., Bull, P.C., Conway, D.J., Marsh, K., 2010.
1150 Allele-specific antibodies to Plasmodium falciparum merozoite surface protein-2 and protection
1151 against clinical malaria. Parasite Immunol 32, 193–201. https://doi.org/10.1111/j.1365-
1152 3024.2009.01178.x

1153 Peng, D., Tarleton, R., 2015. EuPaGDT: a web tool tailored to design CRISPR guide RNAs for eukaryotic
1154 pathogens. Microb Genom 1. https://doi.org/10.1099/mgen.0.000033

1155 Persson, K.E.M., Fowkes, F.J.I., McCallum, F.J., Gicheru, N., Reiling, L., Richards, J.S., Wilson, D.W.,
1156 Lopaticki, S., Cowman, A.F., Marsh, K., Beeson, J.G., 2013. Erythrocyte-Binding Antigens of
1157 Plasmodium falciparum Are Targets of Human Inhibitory Antibodies and Function To Evade
1158 Naturally Acquired Immunity. The Journal of Immunology 191, 785–794.
1159 https://doi.org/10.4049/jimmunol.1300444

1160 Persson, K.E.M., McCallum, F.J., Reiling, L., Lister, N.A., Stubbs, J., Cowman, A.F., Marsh, K., Beeson,
1161 J.G., 2008. Variation in use of erythrocyte invasion pathways by Plasmodium
1162 falciparum mediates evasion of human inhibitory antibodies. J Clin Invest 118, 342–351.
1163 https://doi.org/10.1172/JCI32138

1164 Reiling, L., Boyle, M.J., White, M.T., Wilson, D.W., Feng, G., Weaver, R., Opi, D.H., Persson, K.E.M.,
1165 Richards, J.S., Siba, P.M., Fowkes, F.J.I., Takashima, E., Tsuboi, T., Mueller, I., Beeson, J.G., 2019.
1166 Targets of complement-fixing antibodies in protective immunity against malaria in children. Nat
1167 Commun 10, 610. https://doi.org/10.1038/s41467-019-08528-z

1168 Ressurreição, M., Thomas, J.A., Nofal, S.D., Flueck, C., Moon, R.W., Baker, D.A., van Ooij, C., 2020. Use
1169 of a highly specific kinase inhibitor for rapid, simple and precise synchronization of Plasmodium
1170 falciparum and Plasmodium knowlesi asexual blood-stage parasites. PLoS One 15, e0235798.
1171 https://doi.org/10.1371/journal.pone.0235798

1172 Richards, J.S., Arumugam, T.U., Reiling, L., Healer, J., Hodder, A.N., Fowkes, F.J.I., Cross, N., Langer, C.,
1173 Takeo, S., Uboldi, A.D., Thompson, J.K., Gilson, P.R., Coppel, R.L., Siba, P.M., King, C.L., Torii, M.,
1174 Chitnis, C.E., Narum, D.L., Mueller, I., Crabb, B.S., Cowman, A.F., Tsuboi, T., Beeson, J.G., 2013.
1175 Identification and Prioritization of Merozoite Antigens as Targets of Protective Human Immunity
1176 to Plasmodium falciparum Malaria for Vaccine and Biomarker Development. The Journal of
1177 Immunology 191, 795 LP – 809.

1178 RTSS Clinical Trials Partnership, 2015. Efficacy and safety of RTS,S/AS01 malaria vaccine with or
1179 without a booster dose in infants and children in Africa: final results of a phase 3, individually

1180 randomised, controlled trial. Lancet 386, 31–45.
1181 https://doi.org/http://dx.doi.org/10.1016/S0140-6736(15)60721-8

1182 Sagara, I., Dicko, A., Ellis, R.D., Fay, M.P., Diawara, S.I., Assadou, M.H., Sissoko, M.S., Kone, M., Diallo,
1183 A.I., Saye, R., Guindo, M.A., Kante, O., Niambele, M.B., Miura, K., Mullen, G.E.D., Pierce, M.,
1184 Martin, L.B., Dolo, A., Diallo, D.A., Doumbo, O.K., Miller, L.H., Saul, A., 2009. A randomized
1185 controlled phase 2 trial of the blood stage AMA1-C1/Alhydrogel malaria vaccine in children in
1186 Mali. Vaccine 27, 3090–3098. https://doi.org/10.1016/j.vaccine.2009.03.014

1187 Salanti, A., Staalsoe, T., Lavstsen, T., Jensen, A.T.R., Sowa, M.P.K., Arnot, D.E., Hviid, L., Theander, T.G.,
1188 2003. Selective upregulation of a single distinctly structured var gene in chondroitin sulphate A-
1189 adhering Plasmodium falciparum involved in pregnancy-associated malaria. Mol Microbiol 49,
1190 179–191. https://doi.org/10.1046/j.1365-2958.2003.03570.x

1191 Sanders, P.R., Kats, L.M., Drew, D.R., O'Donnell, R.A., O'Neill, M., Maier, A.G., Coppel, R.L., Crabb, B.S.,
1192 2006. A Set of Glycosylphosphatidyl Inositol-Anchored Membrane Proteins of Plasmodium
1193 falciparum Is Refractory to Genetic Deletion. Infect Immun 74, 4330–4338.
1194 https://doi.org/10.1128/IAI.00054-06

1195 Scally, S.W., Triglia, T., Evelyn, C., Seager, B.A., Pasternak, M., Lim, P.S., Healer, J., Geoghegan, N.D.,
1196 Adair, A., Tham, W.-H., Dagley, L.F., Rogers, K.L., Cowman, A.F., 2022. PCRCR complex is essential
1197 for invasion of human erythrocytes by Plasmodium falciparum. Nat Microbiol 7, 2039–2053.
1198 https://doi.org/10.1038/s41564-022-01261-2

1199 Sheehy, S.H., Duncan, C.J.A., Elias, S.C., Choudhary, P., Biswas, S., Halstead, F.D., Collins, K.A., Edwards,
1200 N.J., Douglas, A.D., Anagnostou, N.A., Ewer, K.J., Havelock, T., Mahungu, T., Bliss, C.M., Miura,
1201 K., Poulton, I.D., Lillie, P.J., Antrobus, R.D., Berrie, E., Moyle, S., Gantlett, K., Colloca, S., Cortese,
1202 R., Long, C.A., Sinden, R.E., Gilbert, S.C., Lawrie, A.M., Doherty, T., Faust, S.N., Nicosia, A., Hill,
1203 A.V.S., Draper, S.J., 2012. ChAd63-MVA-vectored blood-stage malaria vaccines targeting MSP1
1204 and AMA1: assessment of efficacy against mosquito bite challenge in humans. Mol Ther 20,
1205 2355–2368. https://doi.org/10.1038/mt.2012.223

1206 Smythe, J.A., Coppel, R.L., Day, K.P., Martin, R.K., Oduola, A.M., Kemp, D.J., Anders, R.F., 1991.
1207 Structural diversity in the Plasmodium falciparum merozoite surface antigen 2. Proceedings of
1208 the National Academy of Sciences 88, 1751 LP – 1755. https://doi.org/10.1073/pnas.88.5.1751

1209 Srinivasan, P., Beatty, W.L., Diouf, A., Herrera, R., Ambroggio, X., Moch, J.K., Tyler, J.S., Narum, D.L.,
1210 Pierce, S.K., Boothroyd, J.C., Haynes, J.D., Miller, L.H., 2011. Binding of Plasmodium merozoite

1211 proteins RON2 and AMA1 triggers commitment to invasion. Proceedings of the National
1212 Academy of Sciences 108, 13275–13280. https://doi.org/10.1073/pnas.1110303108

1213 Stanisic, D.I., Richards, J.S., McCallum, F.J., Michon, P., King, C.L., Schoepflin, S., Gilson, P.R., Murphy,
1214 V.J., Anders, R.F., Mueller, I., Beeson, J.G., 2009. Immunoglobulin G Subclass-Specific Responses
1215 against Plasmodium falciparum Merozoite Antigens Are Associated with Control of Parasitemia
1216 and Protection from Symptomatic Illness. Infect Immun 77, 1165–1174.
1217 https://doi.org/10.1128/IAI.01129-08

1218 Stejskal, L., Kalemera, M.D., Lewis, C.B., Palor, M., Walker, L., Daviter, T., Lees, W.D., Moss, D.S.,
1219 Kremyda-Vlachou, M., Kozlakidis, Z., Gallo, G., Bailey, D., Rosenberg, W., Illingworth, C.J.R.,
1220 Shepherd, A.J., Grove, J., 2022. An entropic safety catch controls hepatitis C virus entry and
1221 antibody resistance. Elife 11. https://doi.org/10.7554/eLife.71854

1222 Tamura, K., Stecher, G., Kumar, S., 2021. MEGA11: Molecular Evolutionary Genetics Analysis Version
1223 11. Mol Biol Evol 38, 3022–3027. https://doi.org/10.1093/molbev/msab120

1224 Taylor, H.M., McRobert, L., Grainger, M., Sicard, A., Dluzewski, A.R., Hopp, C.S., Holder, A.A., Baker,
1225 D.A., 2010. The malaria parasite cyclic GMP-dependent protein kinase plays a central role in
1226 blood-stage schizogony. Eukaryot Cell 9, 37–45. https://doi.org/10.1128/EC.00186-09

1227 Thera, M.A., Doumbo, O.K., Coulibaly, D., Laurens, M.B., Ouattara, A., Kone, A.K., Guindo, A.B., Traore,
1228 K., Traore, I., Kouriba, B., Diallo, D.A., Diarra, I., Daou, M., Dolo, A., Tolo, Y., Sissoko, M.S.,
1229 Niangaly, A., Sissoko, M., Takala-Harrison, S., Lyke, K.E., Wu, Y., Blackwelder, W.C., Godeaux, O.,
1230 Vekemans, J., Dubois, M.-C., Ballou, W.R., Cohen, J., Thompson, D., Dube, T., Soisson, L., Diggs,
1231 C.L., House, B., Lanar, D.E., Dutta, S., Heppner, D.G., Plowe, C. V., 2011. A Field Trial to Assess a
1232 Blood-Stage Malaria Vaccine. New England Journal of Medicine 365, 1004–1013.
1233 https://doi.org/10.1056/NEJMoa1008115

1234 Weiss, G.E., Gilson, P.R., Taechalertpaisarn, T., Tham, W.-H.H., de Jong, N.W.M.M., Harvey, K.L.,
1235 Fowkes, F.J.I.I., Barlow, P.N., Rayner, J.C., Wright, G.J., Cowman, A.F., Crabb, B.S., 2015. Revealing
1236 the Sequence and Resulting Cellular Morphology of Receptor-Ligand Interactions during
1237 Plasmodium falciparum Invasion of Erythrocytes. PLoS Pathog 11, 284–295.
1238 https://doi.org/10.1371/journal.ppat.1004670

1239 Wickham, H., 2016. ggplot2: Elegant Graphics for Data Analysis. Springer-Verlag New York.

1240 Wilson, D.W., Goodman, C.D., Sleebs, B.E., Weiss, G.E., de Jong, N.W.M., Angrisano, F., Langer, C.,
1241 Baum, J., Crabb, B.S., Gilson, P.R., McFadden, G.I., Beeson, J.G., 2015. Macrolides rapidly inhibit

1242 red blood cell invasion by the human malaria parasite, Plasmodium falciparum. BMC Biol 13, 52.
1243 https://doi.org/10.1186/s12915-015-0162-0

1244 World Health Organization, 2024. World malaria report 2024: addressing inequity in the global malaria
1245 response. World Health Organization, Geneva.

1246 Yang, X., Adda, C.G., MacRaild, C.A., Low, A., Zhang, X., Zeng, W., Jackson, D.C., Anders, R.F., Norton,
1247 R.S., 2010. Identification of key residues involved in fibril formation by the conserved N-terminal
1248 region of Plasmodium falciparum merozoite surface protein 2 (MSP2). Biochimie 92, 1287–95.
1249 https://doi.org/10.1016/j.biochi.2010.06.001

1250 Zerebinski, J., Margerie, L., Han, N.S., Moll, M., Ritvos, M., Jahnmatz, P., Ahlborg, N., Ngasala, B.,
1251 Rooth, I., Sjöberg, R., Sundling, C., Yman, V., Färnert, A., Plaza, D.F., 2024. Naturally acquired IgG
1252 responses to Plasmodium falciparum do not target the conserved termini of the malaria vaccine
1253 candidate Merozoite Surface Protein 2. Front Immunol 15, 1501700.
1254 https://doi.org/10.3389/fimmu.2024.1501700

1255 Zhang, X., Adda, C.G., Low, A., Zhang, J., Zhang, W., Sun, H., Tu, X., Anders, R.F., Norton, R.S., 2012.
1256 Role of the helical structure of the N-terminal region of plasmodium falciparum merozoite
1257 surface protein 2 in fibril formation and membrane interaction. Biochemistry 51, 1380–1387.
1258 https://doi.org/10.1021/bi201880s

1259 Zhang, X., Perugini, M.A., Yao, S., Adda, C.G., Murphy, V.J., Low, A., Anders, R.F., Norton, R.S., 2008.
1260 Solution conformation, backbone dynamics and lipid interactions of the intrinsically
1261 unstructured malaria surface protein MSP2. J Mol Biol 379, 105–21.
1262 https://doi.org/10.1016/j.jmb.2008.03.039

1263

Table 1. Amino acids sequence properties for the N and C-terminal conserved, and N-terminal repeat, regions for available *P. falciparum* 3D7, *Laverania* (including 3 *Laverania* sequences of unknown speciation) *P. relictum* and *P. gallinaceum* MSP2 sequences.

	N terminal				Repeat regions						C terminal			
Species	Polar uncharged	Basic	Acidic	Hydrophobic	% G	% S	% T	% A	Number of repeats	Amino acid range	Polar uncharged	Basic	Acidic	Hydrophobic
P. falciparum 3D7	50%	17%	4%	29%	50%	25%	0%	25%	6	54-77	46%	16%	10%	28%
P. praefalciparum G01	54%	17%	4%	25%	29%	7%	43%	7%	2	62-75	48%	16%	12%	24%
P. reichenowi CDC	54%	17%	4%	25%	36%	24%	18%	13%	3+4^	51-105	48%	16%	12%	24%
P. reichenowi G01	54%	17%	4%	25%	33%	0%	33%	33%	5	67-81	48%	16%	12%	24%
P. reichenowi XM_012905494.2	54%	17%	4%	25%	29%	0%	29%	38%	6*	67-87	48%	16%	12%	24%
P. billcollinsi G01	54%	17%	4%	25%	31%	6%	25%	13%	4*	53-68	52%	18%	10%	20%
P. blacklocki G01	50%	21%	4%	25%	23%	31%	31%	8%	4*	52-64	40%	16%	16%	28%
P. adleri G01	50%	17%	4%	29%	19%	19%	25%	11%	5*	45-80	44%	10%	12%	34%
P. gaboni SY75	46%	17%	8%	29%	21%	33%	21%	17%	6	61-84	45%	12%	10%	33%
P. relictum	54%	13%	4%	29%	33%	0%	33%	33%	8	57-80	33%	12%	22%	33%
P. gallinaceum 8A	38%	25%	4%	33%	31%	6%	19%	25%	4*	55-70	33%	8%	25%	34%
Plasmodium sp. 1 MAP-2013 JX899678	50%	17%	4%	29%	26%	4%	30%	22%	4*	51-73	48%	16%	12%	24%
Plasmodium sp. 2 MAP-2013 JX893169	50%	17%	4%	29%	26%	4%	30%	22%	4*	55-77	48%	16%	12%	24%
Plasmodium sp. 2 MAP-2013 JX893170	46%	21%	4%	29%	25%	6%	31%	19%	4*	51-66	48%	16%	12%	24%

	Conservation of amino acids between repeats
Full	100% conservation of amino acid composition and positions
Partially degenerate	81-99% conservation of amino acid composition (between all pairs of repeats); full conservation of amino acid positions
Degenerate	50-80% conservation of amino acid composition in partially conserved positions (between all pairs of repeats)
Highly degenerate	50-80% conservation of amino acid composition to that in one selected repeat; no conservation of amino acid positions

*insertion present
^two repeat sequences

Table 2: Genes significantly up or down-regulated with Pf3D7 MSP2 KO

Gene Name	log2FoldChange	p-value	Name
PF3D7_0202400	2.547546545	1.09E-36	translation-enhancing factor
PF3D7_1348000	1.604559487	0.000176	conserved Plasmodium protein, unknown function
PF3D7_1423500	1.411878628	4.31E-08	conserved Plasmodium protein, unknown function
PF3D7_1208200	1.384846624	3.59E-05	cysteine repeat modular protein 3
PF3D7_1461800	1.376899732	9.97E-05	conserved Plasmodium protein, unknown function
PF3D7_0909100	1.155215486	4.07E-05	conserved Plasmodium membrane protein, unknown function
PF3D7_1426500	1.021678659	1.52E-05	ABC transporter G family member 2
PF3D7_0322200	1.014455112	0.000313	conserved protein, unknown function
PF3D7_1372100	-2.436194076	9.31E-18	Plasmodium exported protein (PHISTb), unknown function
PF3D7_1149400	-2.748153616	1.72E-25	Plasmodium exported protein, unknown function
PF3D7_0206800	-4.324734054	9.44E-13	merozoite surface protein 2

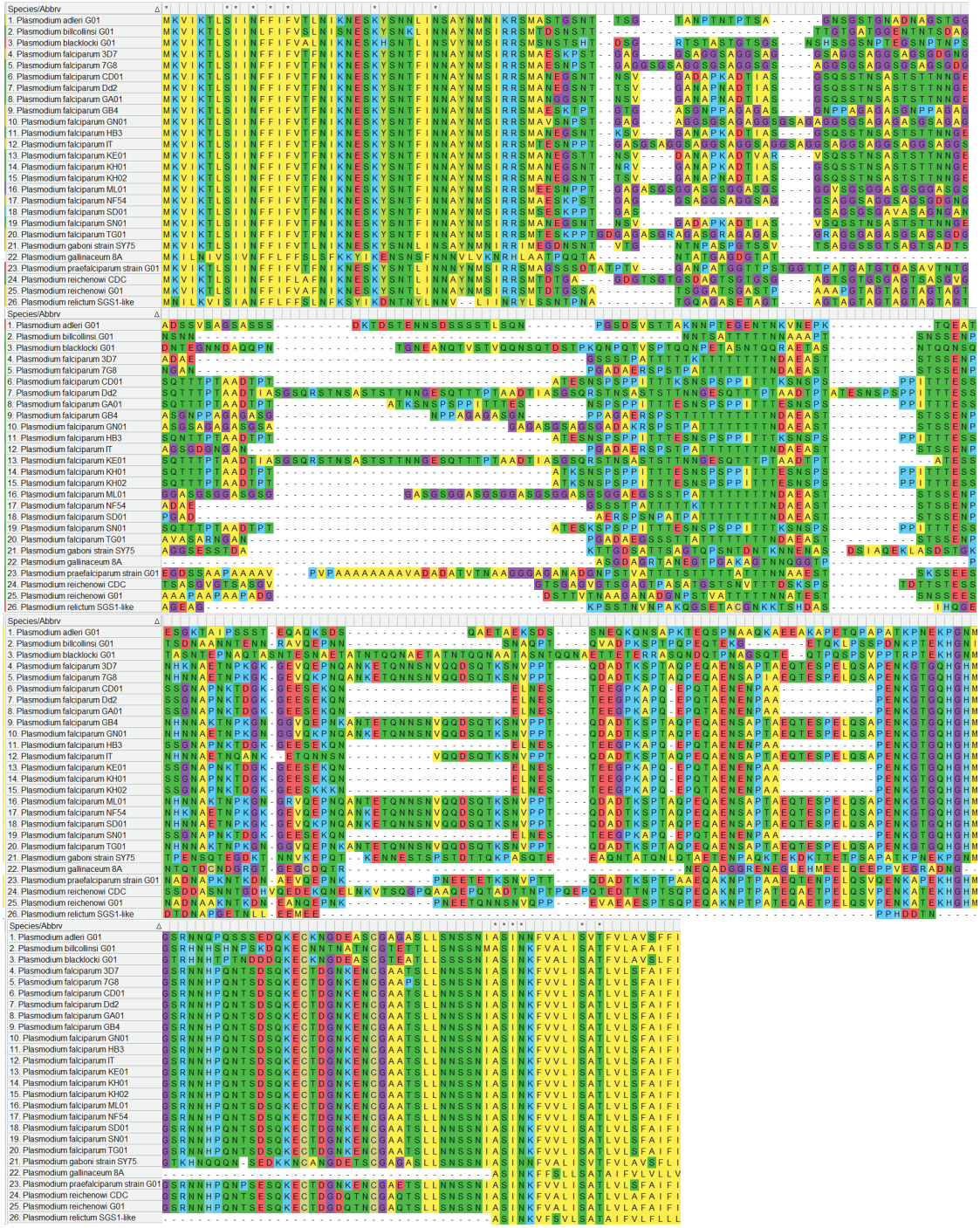

Supplementary Figure 1 Alignment of full-length amino acid protein sequences for all *Pf*MSP2 like sequences on PlasmoDB. Alignment done using MUSCLE alignment with default settings.

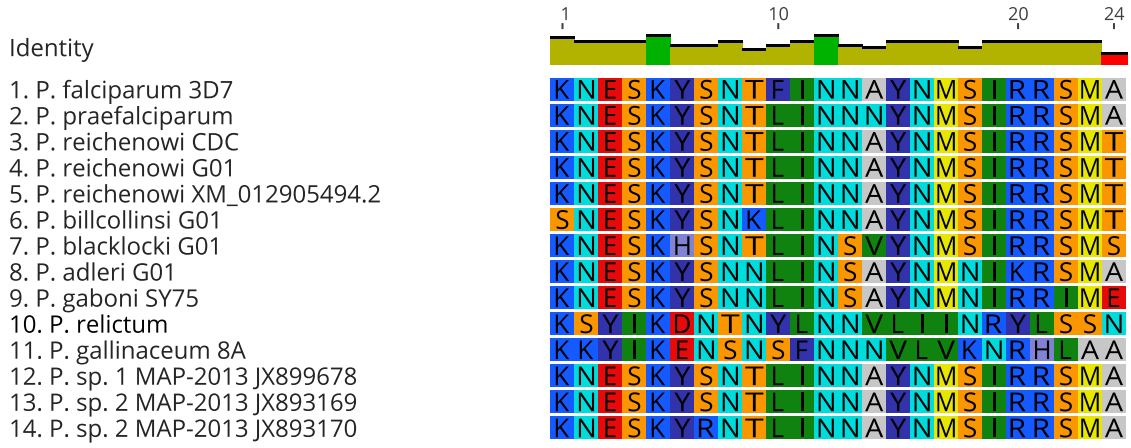

Supplementary Figure 2 Alignment (Blosum 62) of Amino acid sequences for the N-terminal conserved region of *P. falciparum* 3D7, available *Laverania*, *P. relictum* and *P. gallinaceum* MSP2 like sequences on PlasmoDB and identified through a BLAST search on the NCBI server. P. sp. 1, 2 and 3 represent MSP2 sequences identified using a BLAST search that are indicated to be from an unspecified *Laverania* spp. parasite. Amino acids are coloured according to their properties (RasMol).

Supplementary Figure 3 Amino Acid sequences for the N-terminal repeat region of *P. falciparum* 3D7, available *Laverania*, *P. relictum* and *P. gallinaceum* MSP2 like sequences on PlasmoDB and identified through a BLAST search on the NCBI server. P. sp. 1, 2 and 3 represent MSP2 sequences identified using a BLAST search that are indicated to be from an unspecific *Laverania* spp. parasite. Sequences presented are not aligned, with the exceptions of the 3 *P. reichenowi* and 3 unspecified *Laverania* sequences in order to highlight the conserved sequence despite an insertion. Insertions that are considered to break up the small amino acid and/or repeat structure for the purposes of this comparison are underlined in Black. Respeats, both conserved and degenerate, are underlined in grey. Amino acids are coloured according to their properties (RasMol).

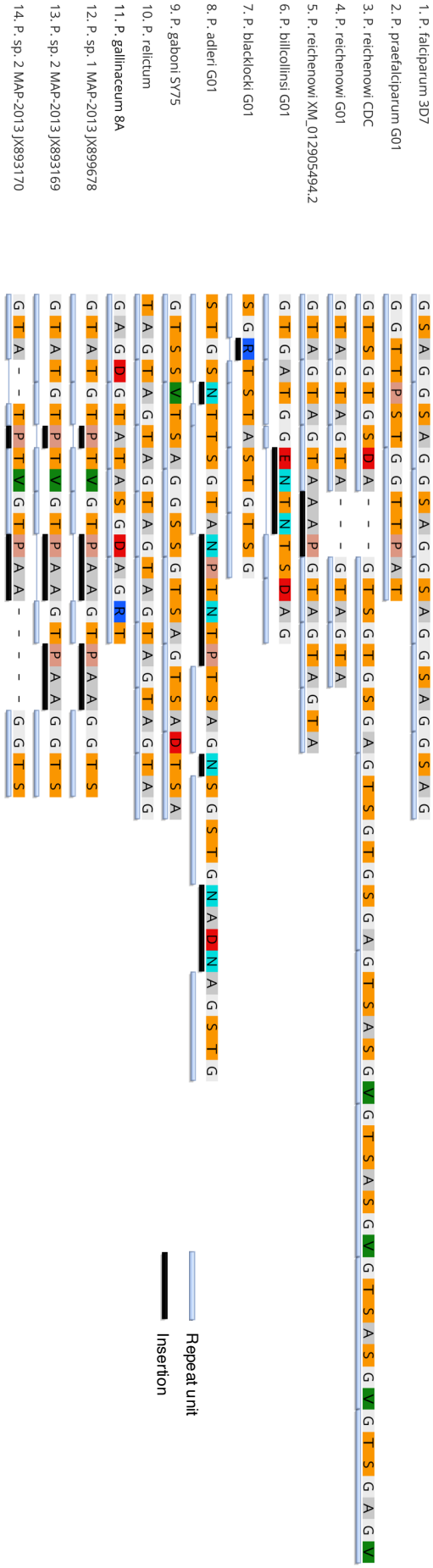

Supplementary Figure 4 Alignment of amino acid sequences for the region corresponding to the C-terminal conserved region of *P. falciparum* 3D7, available *Laverania*, *P. relictum* and *P. gallinaceum* MSP2 like sequences on PlasmoDB and identified through a BLAST search on the NCBI server. *P. sp.* 1, 2 and 3 represent MSP2 sequences identified using a BLAST search that are indicated to be from an unspecified *Laverania* spp. parasite. Initial alignment done using Blosum62 with default settings, with subsequent manual modification as required to align to the cysteine residues and other prominent areas of conservation between the *Laverania* and avian malarias. Amino acids are coloured according to their properties (RasMol).

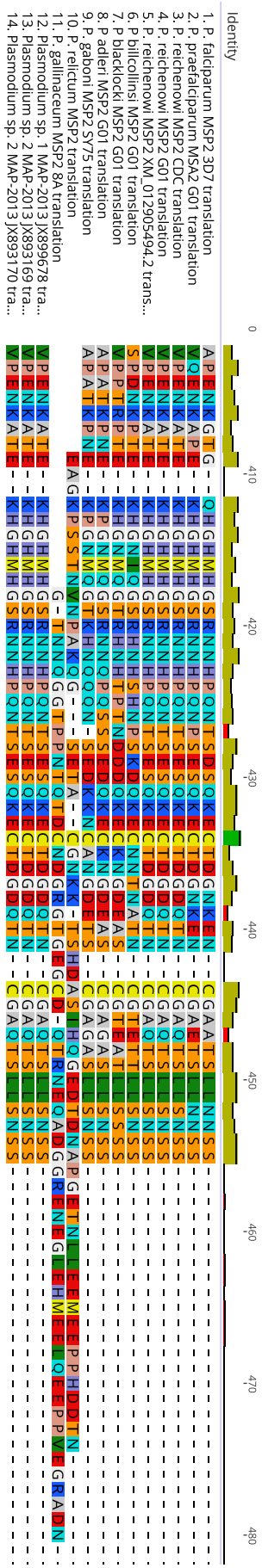

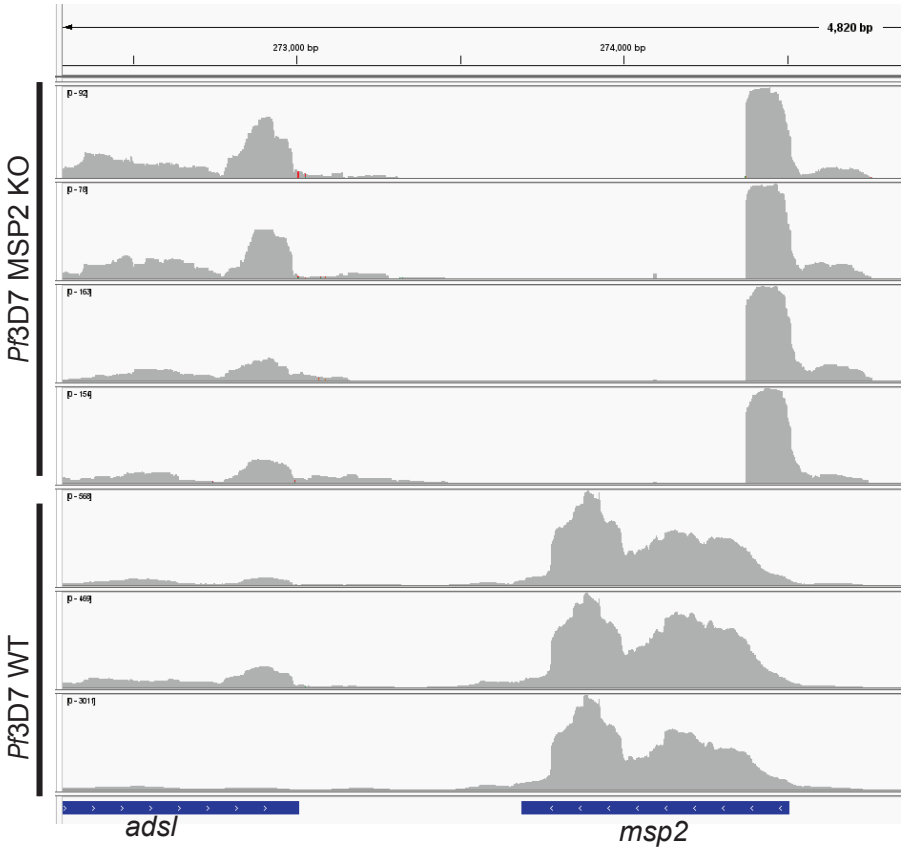

Supplementary Figure 5 Coverage plot (IGV) showing absence of majority of *msp2* in schizont transcriptome of *Pf*3D7 DMSP2 parasites but *msp2* presence in *Pf*3D7 MSP2WT. Small section of *msp2* transcribe in *Pf*3D7 ΔMSP2 parasites corresponds with the end of the homology region and primarily covers the signal peptide.

Supplementary Table 1. Primers used to generate MSP2 KO lines.

5' flank MSP2 KO F	GGTCCGCGGCTCGACTAATCAATTTACAATTTC	Sac11
5' flank MSP2 KO R	GGTACTAGTGCCATACTTCTCCTTATACTC	Spe1
3' flank MSP2 KO F	GGTGAATTCCTCTTCATTTTAAAACATTGAC	Ecor1
3' flank MSP2 KO R	GGTCCATGGGTTTTTTCAATGCGTGC	Nco1
Dd2 MSP2 KO 5' flank F	GGTCCGCGGCTCGACTAATCAATTTACAATTTCC	Sac11
Dd2 MSP2 KO 5' flank R	GGTACTAGTCTAGTAGTATTAGAACCTTCATTTG	Spe1
Dd2 MSP2 KO 3' flank F	GGTGAATTCATTCTCTTCATTTTAAAACATTGAC	EcoR1
Dd2 MSP2 KO 3' flank R	GGTCCATGGGTACTTGAAGAAATATGGTACC	Nco1
PfMSP2 guide 1 F	TAAGTATATAATATTTGGTAATGGTGCAGATGCTGGTTTT AGAGCTAGAA	
PfMSP2 guide 1 R	TTCTAGCTCTAAAACCAGCATCTGCACCATTACCAAATATT ATATACTTA	
Dd2 MSP2 Guide 2 F	TAAGTATATAATATTGCACCAGAGAATAAAGGTACGTTTT AGAGCTAGAA	
Dd2 MSP2 Guide 2 R	TTCTAGCTCTAAAACGTACCTTTATTCTCTGGTGCAATAT TATATACTTA	
5' int 3D7 MSP2 KO F	CTTTTCATATAATAAATCAAATGCAC	
5' int 3D7 MSP2 KO R	TACAAAATGCTTAAGACAGATC	
3D7 WT 5' int check R	GGTAGTTGTGGTAGTAGC	
Dd2 5' check F	CAATTACGATATAAAACCTAGTATCTTTC	
Dd2 WT 5' int check R	CTATTTGTACTCCTTTGACTTCCAC	

Supplementary Table 2. Antibodies used in this study.

Serum/Antibody/ibody	Source
Anti-MSP2 mAb 2F2	Adda et al Infect Immun 2012
Anti-MSP2 Rb FC27	Robin Anders, LaTrobe University
Anti-EXP2 Rb	Bullen et al. J Biol Chem 2012
Anti-PfAldolase	Abcam
Anti-PfRh2b Rb 1055-3	Lopaticki et al Infect and Immun 2011
Anti-PfEBA175/Rh2b Rb 1056-3	Lopaticki et al Infect and Immun 2011
Anti-PfEBA175/Rh4 Rb 1049-3	Lopaticki et al Infect and Immun 2011
Anti-PfEBA175/Rh2b/Rh4 Rb 1067-3	Lopaticki et al Infect and Immun 2011
Anti-w2mef EBA175 Rb	Healer et al PLoS One 2013
Anti-MSP1-19 Rb (6858, 645, 647)	Paul Gilson, Burnet Institute
Anti-Rh5.1 Rt 494	Healer et al Front Cell Infect Microbiol 2022
Anti-PTRAMP nAb H8	Scally et al Nat Microbiol 2022
Anti-CSS nAb D2	Scally et al Nat Microbiol 2022
Anti-CSS nAb D2-FC	Scally et al Nat Microbiol 2022
Anti-AMA1 3D7 Rb (1072, 1149, 1161)	Drew et al. PLoS One 2012
Anti-AMA1 w2mef Rb (1151, 1164, 1163, 128/7)	Drew et al. PLoS One 2012
Anti-AMA1 mAb 1F9	Coley et al PEDS 2001
Anti-AMA1 mAb 4G2	Collins et al J. Biol. Chem. 2007
Anti-AMA1 ibody WD33	Angange et al Under Review
Anti-AMA1 ibody WD34	Angange et al Under Review
Anti-AMA1 WD34	Angange et al Under Review
Anti-AMA1 ibody WD34-FC	Angange et al Under Review

Rb= rabbit. mAb= mouse monoclonal. Rt= rat. nAb= camelid nanobody. I-body= single domain antibody derived from shark variable new antigen receptor (V_{NAR}).

Supplementary Table 3. Enzymes used to remove/inactivate RBC receptors and target residues of the enzyme.

Enzyme	Cleavage Target	Supplier
Neuraminidase (0.067 U/mL)	Sialic acid residues	Sigma-Aldrich
High Trypsin (1 mg/mL)	Lysine or Arginine residues, unless followed by a proline	Sigma-Aldrich
Low Trypsin (0.067 mg/mL)	Lysine or Arginine residues, unless followed by a proline	Sigma-Aldrich
Chymotrypsin (1 mg/mL)	Tyrosine, Tryptophan or Phenylalanine	Worthington Biochemical Corporation
Chymotrypsin (1 mg/mL)/ Trypsin (0.067 mg/mL)	Tyrosine, Tryptophan, Phenylalanine, Lysine or Arginine residues, unless followed by a proline	Worthington Biochemical Corporation & Sigma-Aldrich

Supplementary Table 4. Primers used for RT- qPCR of *P. falciparum* MSP2, MSP5, MSP4 and controls.

Name	Sequence
FrucBiAld 3D7 F qPCR [a, b]	TGTACCACCAGCCTTACCAG
FrucBiAld 3D7 R qPCR [a,b]	TTCCTTGCCATGTGTTCAAT
MSP2 3D7 F qPCR	TCCTACTGCACAACCTGAACAA
MSP2 3D7 R qPCR	ATGTCCATGTTGTCCTGTACCTT
MSP4 3D7 F qPCR	CAAAAGAATCCCAAATGGTTGATGATAA
MSP4 3D7 R qPCR	AACATGGCCACCTGAATTTGAT
MSP5 3D7 F qPCR	AAATTAATGAGAATGCAGAAATAGGTCAA
MSP5 3D7 R qPCR	CGCTATAATGTGGCACCTCAT
SUB1 3D7 F qPCR[c]	GGAATGAGGTAGATGCCGATGAA
SUB1 3D7 F qPCR[c]	TCCTTTACATCTTTCAGTTCCCTCAT

[a] FrucBisAld primers had been previously validated as an appropriate housekeeping gene by Salanti et. al. (2003). Primers listed here are the fructose-bisphosphate aldolase qPCR primers (primer pair 61) from Salanti et. al. (2003).

[b] fructose-bisphosphate aldolase is ubiquitously expressed throughout the parasite lifecycle and is used as a non-stage specific housekeeping gene.

[c] SUB1 is a schizont expressed protein and is used as a schizont-stage specific housekeeping gene.